Energy 291 (2024) 130415

Contents lists available at ScienceDirect

Energy

journal homepage: www.elsevier.com/locate/energy

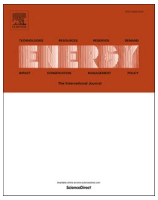

Partial load operation characteristics of supercritical CO_2 coal-fired power generation system

Haonan Zheng [a], Zheng Miao [a,b,*], Jinliang Xu [a,b]

[a] Beijing Key Laboratory of Multiphase Flow and Heat Transfer for Low Grade Energy Utilization, North China Electric Power University, Beijing, 102206, China
[b] Key Laboratory of Power Station Energy Transfer Conversion and System (North China Electric Power University), Ministry of Education, Beijing, 102206, China

ARTICLE INFO

Handling Editor: Dr L Luo

Keywords:
Supercritical CO_2 coal-fired power generation system
Partial load
Control strategy
Burner angle
Split ratios

ABSTRACT

The steady-state model of a 300 MW supercritical CO_2 coal-fired power generation system (SCPGS) is established to investigate its partial load characteristics. The SCPGS model predicts the reduction of reheat CO_2 temperature in partial load operation, which is not reflected from the traditional black box model due to its simplification of heat transfer processes in the boiler. Effects of the burner angle and split ratios on regulating the reheat temperature is simulated. It is found that increasing the burner angle can effectively raise the reheat temperature and system efficiency. However, the higher furnace outlet temperature makes the heating surface easy to coke and slag. Changing the split ratios can also regulate the reheat temperature while the system efficiency is reduced. Accordingly, a comprehensive control strategy is proposed: at 100%–85 % load ratio, no regulation is applied; at 85%–45 % load ratio, the burner angle is gradually adjusted upward; at 45%–20 % load ratio, the burner angle is set to 30^o and the split ratios are changed in the order of x_{EAP}, x_{H4a}, and x_{C2}. This control strategy enables the SCPGS to achieve wide load regulation efficiently and safely and can provide guidance for the dynamic regulation of the SCPGS with variable load operation.

1. Introduction

The world is experiencing the third major energy transition, and global carbon emission is still large and with high growth rates [1]. Many countries are actively adjusting their energy development strategies, striving to reach peak carbon emissions and achieve carbon neutrality [2]. Energy conversion processes should be sped up for clean and effective use. The efficiency of conventional power generation systems is, however, constrained by the limitations of metallic materials under high temperature and pressure conditions [3,4], thus it is urgent to develop new power generation systems to further increase the energy conversion efficiency. The supercritical carbon dioxide Brayton cycle (sCO_2 cycle) is one of the promising techniques, first proposed by Sulzer [5] in 1950, which uses CO_2 as the working fluid instead of water for converting heat into power. In comparison to the traditional steam Rankine cycle, the sCO_2 cycle has lower metal corrosion and higher efficiency. Additionally, its fewer components make the system more compact, which increases its flexibility and makes it better suited for variable load operation and power grid peak regulation [6].

Based on the simple sCO_2 Brayton cycle (SC), scholars investigated various sCO_2 cycle configurations to further increase the sCO_2 cycle's efficiency. In 1968, Feher [7] analyzed SC and concluded that it may be employed in nuclear power generation systems and space power generation systems because of its high efficiency. Later, Angelino [8] proposed the recompression cycle (RC), pre-compression cycle, partial cooling cycle, and other configurations. He found that the sCO_2 cycle was more efficient than the secondary reheated steam Rankine cycle in the high temperature range (650–800 °C). Utamura M [9] examined the internal flow and heat exchange mechanism of the recuperator in the sCO_2 cycle and concluded that RC can effectively avoid the recuperator pinch point problem and make the system more efficient. Researchers have also improved the thermal efficiency of sCO_2 cycle by incorporating the intercooling [10,11] and reheating [12,13] processes into the system. In order to maximize the sCO_2 cycle's compatibility with various heat sources, Chacartegui et al. [14] and Saeb M. Besarati et al. [15] coupled an organic Rankine cycle as the bottom cycle in the sCO_2 solar power production system, which increased the thermal efficiency by 3–7%. Our group developed the multi-stage compression sCO_2 cycle by introducing the synergetics [16] and proposed the overlap energy utilization principle for the coal-fired sCO_2 cycle [17] to maximize the

* Corresponding author. Beijing Key Laboratory of Multiphase Flow and Heat Transfer for Low Grade Energy Utilization, North China Electric Power University, Beijing, 102206, China.
E-mail address: miaozheng1982@hotmail.com (Z. Miao).

https://doi.org/10.1016/j.energy.2024.130415
Received 3 August 2023; Received in revised form 2 January 2024; Accepted 19 January 2024
Available online 27 January 2024

thermal efficiency of sCO_2 coal-fired power generation system (SCPGS). The sCO_2 cycle studies mentioned above primarily concentrate on configuration optimization design to improve the thermal efficiency at design conditions.

Since the actual power generation systems often operate under off-design conditions due to fluctuating heat source characteristics, external disturbances, and changes in grid load requirements, it is necessary to study the off-design performance of sCO_2 cycle power systems. The majority of sCO_2 cycle off-design conditions investigations focus on sCO_2 solar power systems because the external environment has a significant impact on the heat and cold sources in sCO_2 solar power systems. Duniam et al. [18] and Neises [19] suggested that the effect of rising ambient temperature on the system performance can be reduced by varying the compressor speed and optimizing the split ratio and compressor inlet temperature. Singh et al. [20] concluded that in summer, the system power can be made greater than the design power for most of the day by controlling the heat input to the sCO_2 solar power system. At ambient temperatures greater than 30 °C, Chen et al. [21] found less performance penalty for SC and RC compared to complex cycle configurations. When the solar intensity is low, Wang et al. [22] found that the energy storage system can provide some buffering effect.

Due to the load requirements or the characteristics of the heat source, power generation systems frequently operate under partial load conditions. The existing studies on the partial load operation characteristics of the sCO_2 cycle have primarily concentrated on small-scale power production systems under 10 MW, where the systems mostly utilize the centrifugal compressors and radial turbines. Dyreby et al. [23] and Yang et al. [24] examined the partial load performance of a 10 MW sCO_2 cycle with various configurations, Dyreby et al. [23] discovered that as the load ratio is reduced, the thermal efficiency of RC decreases and the SC increases. According to Yang et al.'s research [24], the efficiency of the reheat cycle is least affected by load variation and the recompression and reheat cycle has the best performance when the average daily generation load is below 62.5 %. Li et al. [25] found that the four control methods: inventory control, bypass control, throttling control, and temperature control, can achieve 10%–100 % load regulation for the 5 MW SC power generation system, and the partial load performance of various operation control methods ranges from good to poor. Fan et al. [26,27] and Ahn et al. [28] also claimed that the thermal efficiency of the sCO_2 cycle at partial load is highest under the inventory control method. For the inventory control method, Sathish et al. [29] concluded the worsening of the system's partial load efficiency is caused by the turbine efficiency reduction, while Alfani et al. [30,31] proposed that the smaller efficiency at lower loads is due to the decrease in system pressure ratio.

In the coming decades, coal-fired power generation is expected to remain the dominant source of electricity supply worldwide. The application of sCO_2 cycle to coal-fired power generation systems can improve the system efficiency [32]. The capacity of SCPGS is usually larger than 100 MW so that axial compressor and axial turbine are required to ensure efficiency [33], which is significantly different from the small-scale sCO_2 power production systems. Moreover, in order to realize the large-scale consumption of renewable energy sources, the coal-fired power plants have to change from the base-load power production mode to a flexible and variable back-up power production mode. Therefore, research on the off-design conditions of SCPGS to improve their partial load performance will play an important role in promoting the transition of energy structure. In a limited quantity of literature, the off-design performance of SCPGS has been researched. Bai et al. [34] and Li et al. [35] studied the partial load performance of sCO_2 π-type boiler and circulating fluidized bed boiler, respectively. They did not couple the sCO_2 boiler with the sCO_2 cycle during the calculation. A constant boiler inlet working fluid temperature was assumed, which would lead to a large deviation in the results. Tong et al. [36] examined the effects of coal type, and excess air coefficient on the SCPGS and optimized the off-design performance of SCPGS by altering the sCO_2 boiler arrangement structure, but did not conduct a detailed study on the partial load operation characteristics of the SCPGS and the regulation strategy.

According to the above literature review, there are few studies on the partial load operation characteristics of SCPGS, and there is a gap in research on regulation measures to improve the partial load performance of SCPGS. In this work, we select a SCPGS with the typical capacity of 300 MW to study its partial load operation characteristics and try to answer the following questions: (i) How do the key parameters of SCPGS and sCO_2 boiler vary with load ratio? (ii) What regulation measures can be applied to optimize the partial load operation performance of the SCPGS? (iii) Can a comprehensive regulation strategy be developed to enable efficient and safe operation of the SCPGS under partial load conditions? The results of the study can provide theoretical support for the partial load operation and dynamic regulation of the SCPGS. The novelty and contribution of this paper are as follows: (1) The integrated design of the SCPGS and components as well as the partial load calculation process are proposed by coupling the design and off-design model of components with the sCO_2 cycle model; (2) The partial load characteristics of SCPGS and boiler are studied, and it is found that the decrease of reheat temperature result in the lower system thermal efficiency; (3) Two regulation measures are proposed to improve the partial load performance of SCPGS: adjusting the burner angle and changing the split ratio; (4) A comprehensive regulation strategy combining these two measures is proposed, which can meet the demand for deep peak regulation and safe operation of SCPGS.

The remainder of this paper is organized as follows: Section 2 introduces the model of SCPGS, including the thermodynamic model, component design models, and component off-design computational models; Section 3 presents the results and discussion, focusing on the partial load operation characteristics of SCPGS and sCO_2 boiler, and the regulation optimization of the system; Section 4 is the main conclusions.

2. The sCO_2 coal-fired power generation system

As shown in Fig. 1a, the basic configuration of the SCPGS in this work is a recompression cycle with a primary reheat process (RC + RH) [6], which achieves full temperature absorption of boiler flue gas by applying connected-top-bottom cycle [37]. All the sCO_2 does work in the low-pressure turbine (T2) and then enters the top cycle and the bottom cycle respectively at point 6; the sCO_2 entering the top cycle passes through the high-temperature recuperator 1 (HTR1) and low-temperature recuperator (LTR) in turn to release heat, and then reaches point 8; the sCO_2 entering the bottom cycle passes through the external air preheater (EAP) and high-temperature recuperator 2 (HTR2) and LTR to release heat and reach point 8; the sCO_2 flow is split at point 8, part of it enters the recompressor (C2), and the other flows through the cooler (Cooler 1), the main compressor (C1) and LTR in turn, and then split again after point 3a, part of this flow enters the bottom cycle through HTR2, heater 4a (H4a) and heater 4b (H4b) to absorb heat and reach point 5b; the other enters the top cycle and merges with the C2 compressor outlet sCO_2 and flows into HTR and Heater 1 to absorb heat and the reaches point 5b; the sCO_2 from points 5a and 5b merge at point 5 and enters the high pressure turbine (T1); then enters Heater 2 to absorb heat and the drive the low pressure turbine (T2). The turbines T1 and T2 are installed in a coaxial arrangement and connected to a generator for power generation. Compressors C1 and C2 are each connected to a motor for variable speed operation to ensure the efficiency of the unit. In addition, an inventory tank is arranged between the outlet of compressor C1 and the inlet of the cooler as a buffer to realize variable load operation of the unit by storing or releasing part of the CO_2 when changing the mass flow rate of CO_2.

The heating surface arrangement in the sCO_2 boiler is based on the energy overlap utilization principle to maximize the efficiency of the SCPGS [17]. The sCO_2 mass flow rate through the boiler is 6–8 times higher than the conventional steam boiler at the same capacity, thus a

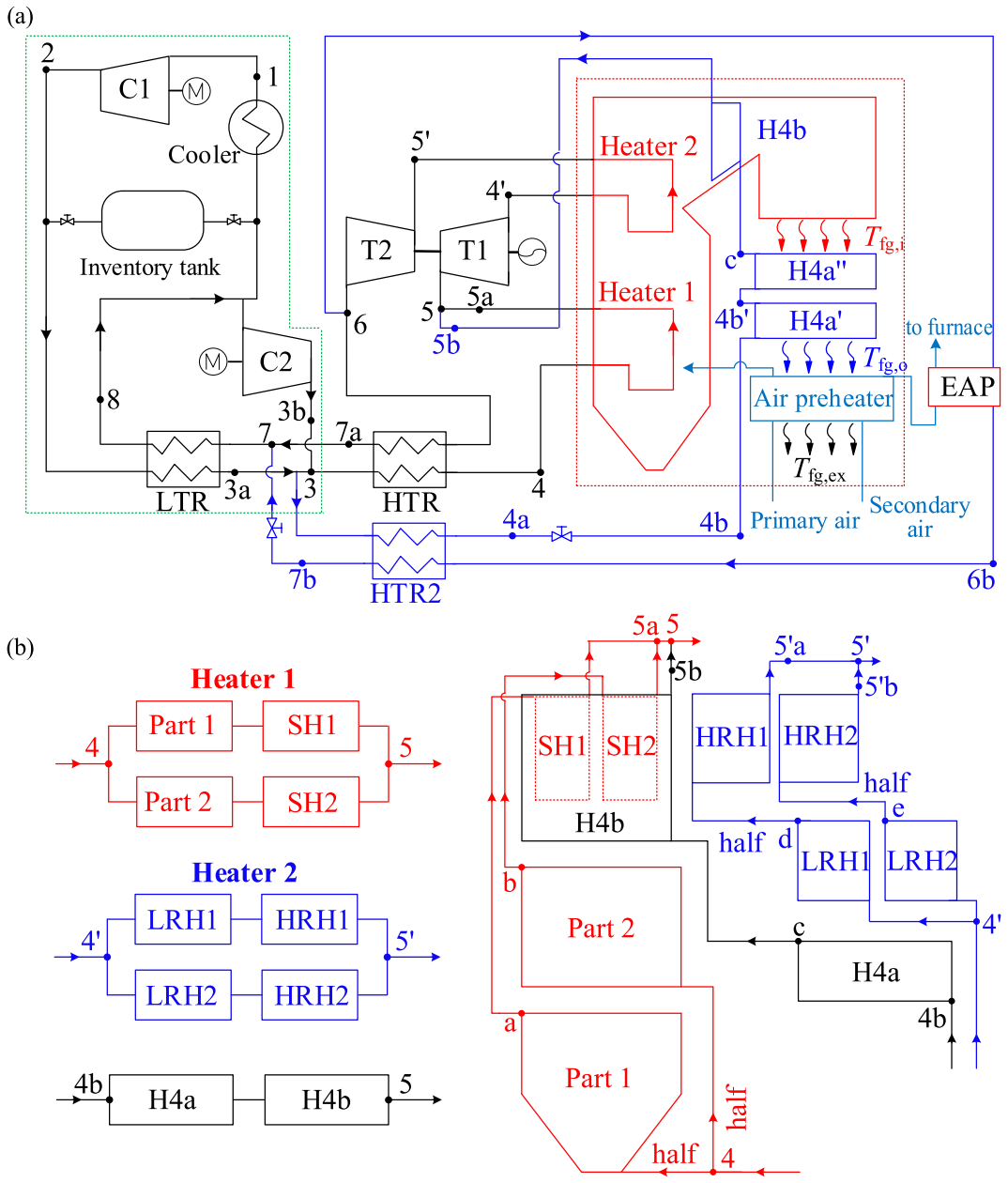

Fig. 1. Configuration of sCO_2 coal-fired power generation system and sCO_2 boiler [6].

large pressure drop is inevitable if the heating surface arrangement in the conventional steam boiler is used. The thermal efficiency of SCPGS is sensitive to the pressure drop of the heater [38]. Consequently, the system in this paper adopts the modular design of the heating surface in partial flow mode to reduce the pressure drop to ~1/8 of the full-flow mode, and the heating surface tube specification can be the same grade as that of the water boiler [6]. As in Fig. 1b, Heater1 consists of Part1+SH1 and Part2+SH2 arranged in parallel, and Heater2 consists of LRH1+HRH1 and LRH2+HRH2 arranged in parallel, the flow rates are equal in the parallel parts.

In this work, a black box model of the sCO_2 power generation system is also developed for comparison, as shown in Fig. 2. The system simulated by the black box model has the same configuration as the SCPGS, except for the heaters. Only two heaters are considered in the black-box model: the main-heater and the Re-heater, and the heat transfer process inside the heaters are ignored. In this way, the CO_2 entering the black-box heaters can be heated to 620 °C at any load ratio by taking account of the conservation of energy [24]. The black box model in thermal systems can simplify the calculation process, therefore it is widely used in the analysis of the conventional steam Rankine cycle [39] and sCO_2 solar power generation systems [24]. We have studied the partial load characteristics of the sCO_2 cycle using the black-box model in the literature [40] and obtained the following findings: (1) When the sCO_2 cycle operates at partial load, there are both positive factors increasing thermal efficiency and negative factors reducing thermal efficiency of the system. The positive factors are the increase in the recuperators effectiveness and the decrease in the pressure drops in each component, whereas the negative factors are the decrease in the main gas pressure and the turbine efficiency. (2) The thermal efficiency of the system increases and then decreases as the load ratio decreases under the combined effect of the positive and negative factors of the partial load operation. The thermal efficiency is greater than the design thermal efficiency at high load ratios (85–100 %), while it is less than the design thermal efficiency at load ratios below 85 %. In the sCO_2 black box model system established in this paper, all components except the heater adopt the same structural size as the SCPGS, and the outlet temperatures

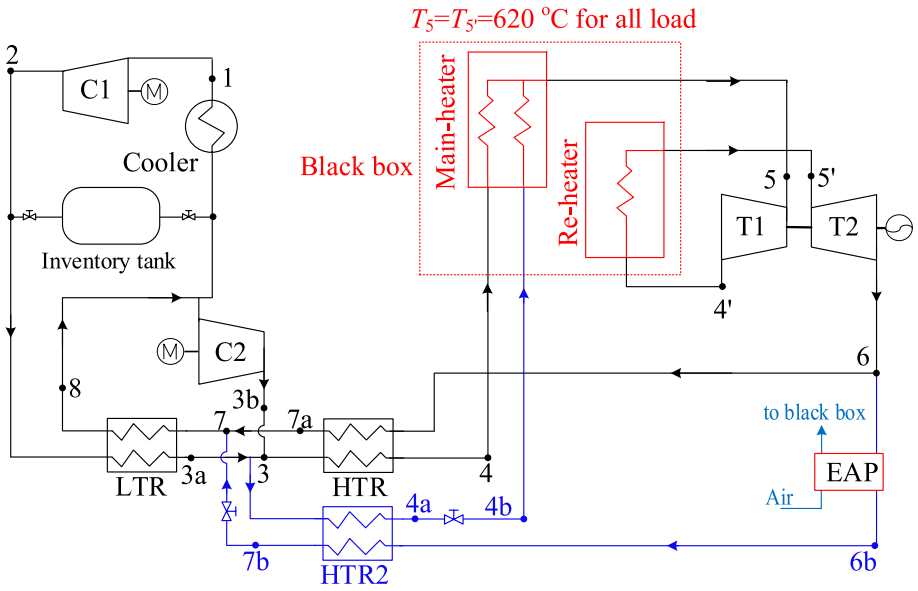

Fig. 2. Configuration of sCO_2 black box model power generation system.

T_5 and $T_{5'}$ of the sCO_2 heated by the Main-Heater and Re-Heater can reach 620 °C at any load ratio.

The assumptions used in the calculation are.

(1) The system partial load performance parameters are calculated during quasi-steady-state operation [24].
(2) The turbines and generator are operated at a constant speed to assure grid security, while the main compressor and recompressor are each connected to a motor for variable speed operation, thus ensuring system flexibility and efficiency [12].
(3) The inlet temperature of T1 is kept constant by adjusting the coal mass flow rate during the partial load operation of the SCPGS [36, 41].
(4) The cooler can provide enough cooling water to keep the constant main compressor inlet condition [26].

2.1. The thermodynamic model

The thermodynamic equations for each component in the system are shown in Table 1 [6], where x_{C2}, x_{H4a}, and x_{EAP} denote the ratio of the mass flow rate of sCO_2 through the recompressor, H4a, and EAP to the total mass flow rate, respectively; the subscript 's' means the isentropic process; η_C and η_T are the isentropic efficiencies of the compressor and turbine; Q and W represent component heat load and power; and H denotes the enthalpy. The net work per unit mass rate of sCO_2, w_{net}, total heat absorption per unit mass rate of CO_2, q_{total}, and thermal efficiency, η_{th}, are expressed as:

$$w_{net} = \frac{W_{T1} + W_{T2} - W_{C1} - W_{C2}}{m_{CO2}} \tag{1}$$

$$q_{total} = (1 - x_{H4a})(H_5 - H_4) + x_{H4a}(H_5 - H_{4b}) + (H_{5'} - H_{4'}) - x_{EAP}(H_6 - H_{6b}) \tag{2}$$

$$\eta_{th} = \frac{w_{net}}{q_{total}} \tag{3}$$

The enthalpy of each merging point in the system is calculated according to the conservation of energy (taking state point 3 as an example):

$$H_3 = H_{3a}(1 - x_{C2}) + H_{3b}x_{C2} \tag{4}$$

Table 1
Thermodynamic equations for components [6].

Components	Thermodynamic equations
C1	$\eta_{C,s} = \frac{H_{2s} - H_1}{H_2 - H_1}$, W_{C1}=(1-x_{C2})(H_2–H_1)m_{CO2}
C2	$\eta_{C,s} = \frac{H_{3bs} - H_8}{H_{3b} - H_8}$, $W_{C2} = x_{C2}(H_{3b}$-$H_8)m_{CO2}$
T1	$\eta_{T1,s} = \frac{H_5 - H_{4'}}{H_5 - H_{4's}}$, W_{T1}=(H_5–$H_{4'}$)m_{CO2}
T2	$\eta_{T2,s} = \frac{H_{5'} - H_6}{H_{5'} - H_{6s}}$, W_{T2}=($H_{5'}$-H_6)m_{CO2}
LTR	$x_{C2} = 1 - \frac{H_7 - H_8}{H_{3a} - H_2}$, Q_{LTR}=(H_7–H_8)m_{CO2}
HTR	$x_{EAP} = 1 - \frac{(1 - x_{H4a})(H_4 - H_3)}{H_6 - H_{7a}}$, Q_{HTR}=(H_6–H_{7a})(1-x_{EAP})m_{CO2}
HTR2	$x_{H4a} = \frac{x_{EAP}(H_{6b} - H_{7b})}{H_{4b} - H_{3a}}$, $Q_{HTR2} = x_{H4a}$ (H_{4b}-H_{3a})m_{CO2}
Cooler	Q_{Cooler}=(1-x_{C2})(H_8–H_1)m_{CO2}
EAP	$Q_{EAP} = x_{EAP}(H_6$–$H_{6b})m_{CO2}$

2.2. Design of components in SCPGS

The structural dimensions of the components do not change during the partial load operation, so the design of the components and the sCO_2 power generation system is the basis for the study of the system's partial load operation characteristics. In this part, the mathematical models for the design of the main components are introduced, and the design parameters of the system and components are carried out to provide the bench for the partial load calculation. Table 2 shows the main thermodynamic parameters for the system and boiler design in this paper.

2.2.1. Printed circuit heat exchangers

The zigzag printed circuit heat exchanger (zigzag-PCHE) shown in Fig. 3 was used for the recuperators and cooler in the cycle, and in the design calculations. Considering the drastic variation of the physical properties of sCO_2, the recuperator is discretized into 20 sub-exchanges to accurately calculate the heat transfer area. Each sub-exchanger is assigned the same heat duty, and its area is calculated by the thermal conductivity-logarithmic mean temperature difference method (UA-LMTD) [42]:

$$L_z = L_c \cos(\alpha) \tag{5}$$

Table 2
Parameters for the cycle computations and boiler design.

Parameter	Values
Net power (W_{net})	300.00 MW
Turbine inlet temperature (T_5, $T_{5'}$)	620.00 °C
Turbine T1 inlet pressure (P_5)	30.00 MPa
Compressor C1 inlet temperature (T_1)	32.00 °C
Compressor C1 inlet pressure (P_1)	7.60 MPa
Turbines isentropic efficiency ($\eta_{T,s}$)	0.93
Compressors isentropic efficiency ($\eta_{C,s}$)	0.89
Pinch temperature difference in LTR/HTR (ΔT)	10.00 °C
Max pressure drop in LTR/HTR/Cooler (ΔP)	0.20 MPa
Pinch temperature difference in Cooler (ΔT_{Cooler})	5.00 °C
Cooling water temperature (T_{water})	25.00 °C
Exhaust gas temperature ($T_{fg,ex}$)	123.00 °C
Environment temperature (T_0)	20.00 °C
Excess air coefficient (α)	1.2
Primary air temperature entering air preheater	31.00 °C
Secondary air temperature entering air preheater	23.00 °C
Ratio of primary air flow rate to the total air flow rate	0.19

$$\frac{m_c\left(H_{c,out}-H_{c,in}\right)}{N}=Q_k=\left|m(H_{k+1}-H_k)\right| \tag{6}$$

$$(UA)_k=\frac{Q_k}{\mathrm{LMTD}_k} \tag{7}$$

$$U_k=\frac{1}{h_{c,k}}+\frac{t_e}{k_{w,k}}+\frac{1}{h_{h,k}R_p} \tag{8}$$

$$t_e(D_c+t_3)=(D_c+t_3)\left(\frac{D_c}{2}+t_2\right)-\frac{\pi {D_c}^2}{8} \tag{9}$$

$$A_k=\frac{1}{2}N_cN_p\left(1+\frac{\pi}{2}\right)D_cL_{c,k} \tag{10}$$

where L_c and α are the channel length and channel angle, in this work, α = 40° is adopted; Q_k is the k-th section heat duty and h is the heat transfer coefficient; R_p is the ratio of the hot side heat exchange plate to the cold side heat exchange plate, $R_p = 2$ is applied for the recuperators while $R_p = 1$ for cooler; t_e is the equivalent thickness of the heat exchange plate. The material of the heat exchange plate is SS316 which has a thermal conductivity $k_w = 13.189 + 0.0153T_w$.

The Nusselt number at the hot and cold sides of the recuperator are calculated by Ref. [42]:

$$Nu=0.0176Re^{0.809}Pr^{1/3}(3000<Re<20600) \tag{11}$$

The Nusslt number for the water side in the cooler is calculated by Ref. [43]:

$$Nu=0.122Re^{0.56}Pr^{0.14} \tag{12}$$

The channel pressure drop is:

$$|P_{k+1}-P_k|=\frac{1}{2}\rho_k{u_k}^2f_k\frac{L_{c,k}}{D_h} \tag{13}$$

where $D_h = \pi D_c/(2+\pi)$ is the hydraulic diameter of the channel.

The friction coefficient f for the CO_2 channel is [42]:

$$f=0.3905Re^{-0.0355}(3000<Re<20600) \tag{14}$$

The friction coefficient f for the water channel is [43]:

$$f=(1.12\ln(Re)+0.85)^{-2} \tag{15}$$

The channel diameter D_c for the recuperators and cooler are 2 mm and 2.2 mm, respectively, and the wall thickness t_2 and the ridge width t_3 are calculated by ASME mechanical design standards [44]. The membrane stress S_m and bending stress S_b of the PCHE heat exchange plate should meet the following rules:

$$S_m<S{\cdot}E,\ S_T<1.5S{\cdot}E \tag{16}$$

where $E = 0.7$ is the joint factor. For the wall thickness t_2:

$$S_m=\frac{PH}{2t_2},S_b=\frac{Ph^2c}{12I_2} \tag{17}$$

$$S_T=S_m+S_b \tag{18}$$

For the ridge width spacing t_3:

$$S_m=\frac{Ph}{t_3},S_b=0 \tag{19}$$

$$S_T=S_m+S_b \tag{20}$$

where S is the allowable stress of the material; for the semicircular channel $h = D_c$, $H = D_c/2$.

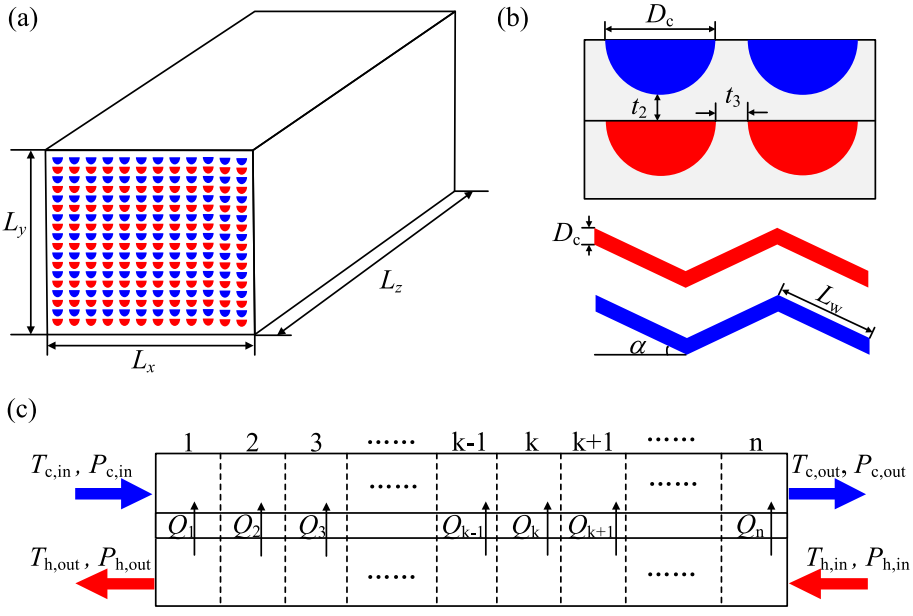

Fig. 3. Geometry of zigzag printed circuit heat exchanger.

2.2.2. Turbomachinery

Since the off-design performance of turbomachinery is closely related to its design parameters, an inverse algorithm is used in the present work to calculate the design parameters of turbomachinery by setting its rated isentropic efficiency, $\eta_{T,s} = 93.00$ % for the turbine and $\eta_{C,s} = 89.00$ % for the compressor, without designing the structural parameters of turbomachinery.

2.2.3. sCO_2 boiler

In the sCO_2 boiler, the burning coal transfers heat to CO_2 by the high temperature flue gas. The coal properties are shown in Table 3 and the coal consumption rate of the boiler m_{coal} is determined by the conservation of energy [6]:

$$m_{coal} = \frac{q_{total} m_{CO2}}{\eta_b Q_f} \tag{21}$$

where Q_f is the heat brought into the boiler per kg of coal; the boiler efficiency $\eta_b = 1\text{-}q_2\text{-}q_3\text{-}q_4\text{-}q_5\text{-}q_6$; q_2, q_3, q_4, q_5, q_6 are heat losses due to exhaust gas, unburned gases loss, unburned carbon loss, radiation, and sensible heat in slag. The heat loss q_2 is calculated by Ref. [45]:

$$q_2 = \left(h_{fg,ex} - h_{ca}\right)(1 - q_4) \,/\, Q_f = \left[h_{fg,ex} - \alpha_{exg} V_0 (ct)_{ca}\right](1 - q_4) \,/\, Q_f \tag{22}$$

where $h_{fg,ex}$ and h_{ca} are the enthalpy of flue gas at the boiler outlet and the enthalpy of the cold air, respectively. α_{exg}, V_0 and $(ct)_{ca}$ are the excess air coefficient, theoretical air volume and the enthalpy per unit volume of cold air.

The heating surfaces in the furnace are Part1, Part2, SH1, SH2 and H4b. The contribution of convective heat transfer in the chamber is less than 5 % therefore only radiation heat transfer is considered. The heat load in the furnace Q_{fur} and the temperature of flue gas at the furnace outlet $T_{fur,o}$ are calculated by Ref. [45]:

$$Q_{fur} = \varphi m_{coal} \left(h_{flame} - h_{fur,o}\right) \tag{23}$$

$$T_{fur,o} = \frac{T_{flame}}{1 + M\left(\varepsilon_{fur}^{syn} \,/\, Bo\right)^{0.6}} \tag{24}$$

where φ is the boiler heat retention coefficient; h_{flame} and T_{flame} are the fuel combustion enthalpy and temperature; $h_{fur,o}$ and $T_{fur,o}$ are the enthalpy and temperature of the flue gas at the furnace outlet; Bo is the Boltzmann number; ε_{fur}^{syn} is the blackness of the furnace flame; M is the parameter characterizing the flame position [45]:

$$M = 0.59 - 0.5(x_B + \Delta x) \tag{25}$$

where x_B is the relative height of the burner; $\Delta x = \pm 0.1$ when the burner is adjusted to $\pm 20^o$, and Δx for other angles is calculated by interpolation.

Based on the conservation of energy, the boiler and heating surface structural parameters are adjusted to meet the following rules:

$$\begin{cases} Q_{fur} = Q_{Part1} + Q_{Part2} + Q_{SH} + Q_{H4b} \\ \varphi m_{coal}\left(h_{fur,o} - h_{fg,ex}\right) = Q_{HRH} + Q_{LRH} + Q_{H4a} + Q_{AP} \end{cases} \tag{26}$$

According to the parameters of sCO_2 cycle and boiler in Table 2, the structural parameters of each component and the parameters of each state point under design conditions can be obtained by coupling thermodynamic and component design models. The integrated design process of SCPGS and components is shown in Fig. 4. The procedure is as followed.

Table 3
Properties of the designed coal.

C_{ar}	H_{ar}	O_{ar}	N_{ar}	S_{ar}	A_{ar}	M_{ar}	V_{daf}	Q_{LHV}
61.70	3.67	8.56	1.12	0.60	8.80	15.55	34.73	23,422

(1) Input the design parameters in Table 2;
(2) Assume the pressure drops in the heaters: $\Delta P^*_{Heater1}$, $\Delta P^*_{Heater2}$;
(3) Assume the pressure drops in the recuperators: ΔP^*_{HTR}, ΔP^*_{LTR} and ΔP^*_{HTR2};
(4) Calculate the state point parameters of the sCO_2 cycle by the thermodynamic model, and determine m_{CO2} according to W_{net};
(5) Input the heat load, mass flow rate and inlet and outlet parameters into the PCHE design program, carry out the mechanical design by the inlet and outlet parameters, then change the heat exchange area to meet the heat load requirements and the pressure drop limit conditions, finally output the calculated PCHE structural parameters and pressure drops ΔP_{HTR}, ΔP_{LTR} and ΔP_{HTR2};
(6) Compare the calculated pressure drops with the assumed values, and return to step (3) if the convergence conditions are not met;
(7) Input the boiler coal properties parameters, loss coefficients $q_1 \sim q_6$, excess air coefficients α, heat load, and tube geometry parameters into the boiler design program, adjust the boiler structural parameters to meet the heat load demand, calculate the pressure drops in the boiler tubes by the thermal-hydraulic model, then output the heater pressure drop $\Delta P_{Heater1}$ and $\Delta P_{Heater2}$;
(8) Compare the calculated heater pressure drops with the assumed values, and return to step (2) if the convergence condition is not satisfied.
(9) When the heater pressure drops meet the convergence conditions, the calculation is completed.

The parameters of each state point under the design conditions of 300 MW SCPGS are shown in Table 4. The structural parameters of boiler heating surfaces are shown in Table 5. The AP consists of two trisection regenerative air preheaters with a rotor inner diameter of 13492 mm, and the specific parameters are shown in Table 6. The system heat exchangers' structural parameters are shown in Table 7. The technical parameters of the turbomachinery under design condition are shown in Table 8.

2.3. Off-design models

2.3.1. Off-design model of heat exchangers

Under off-design conditions, the operating characteristics of the cooler and recuperators in the 300 MW SCPGS are predicted according to the process shown in Fig. 5. Based on the input design parameters of the PCHE as well as the hot and cold side fluid inlet parameter, the pressure drop on both sides and the outlet temperature on the hot side are assumed. Then the heat exchanger is divided into several segments by Q, and the heat transfer area for each segment is calculated. The hot side outlet temperature and the pressure drops on both sides are iteratively updated until the total heat exchanger area A_{cal} and the hot and cold sides pressure drops are converged. The outlet parameters of the PCHE under off-design conditions can be obtained.

2.3.2. Off-design model of compressors

Compared to the radial compressor, the axial compressor has higher efficiency at higher sCO_2 mass flow rates and is more suitable for large-capacity sCO_2 power generation [46]. As the sCO_2 compressors operate near the critical point, the performance is sensitive to changes in the inlet state [47], which acquires high accuracy when speed, mass flow rate, enthalpy rise, and isentropic efficiency are used to describe the compressor performance [48]. Therefore, the ideal gas approach with compressibility correction (IGZ) is used to correct the compressor performance curve parameters for different inlet states [48]. The axial compressor model in this work is derived from the main compressor and recompressor performance curves in the literature [49]. As shown in Fig. 6, the compressor performance curves described in the literature

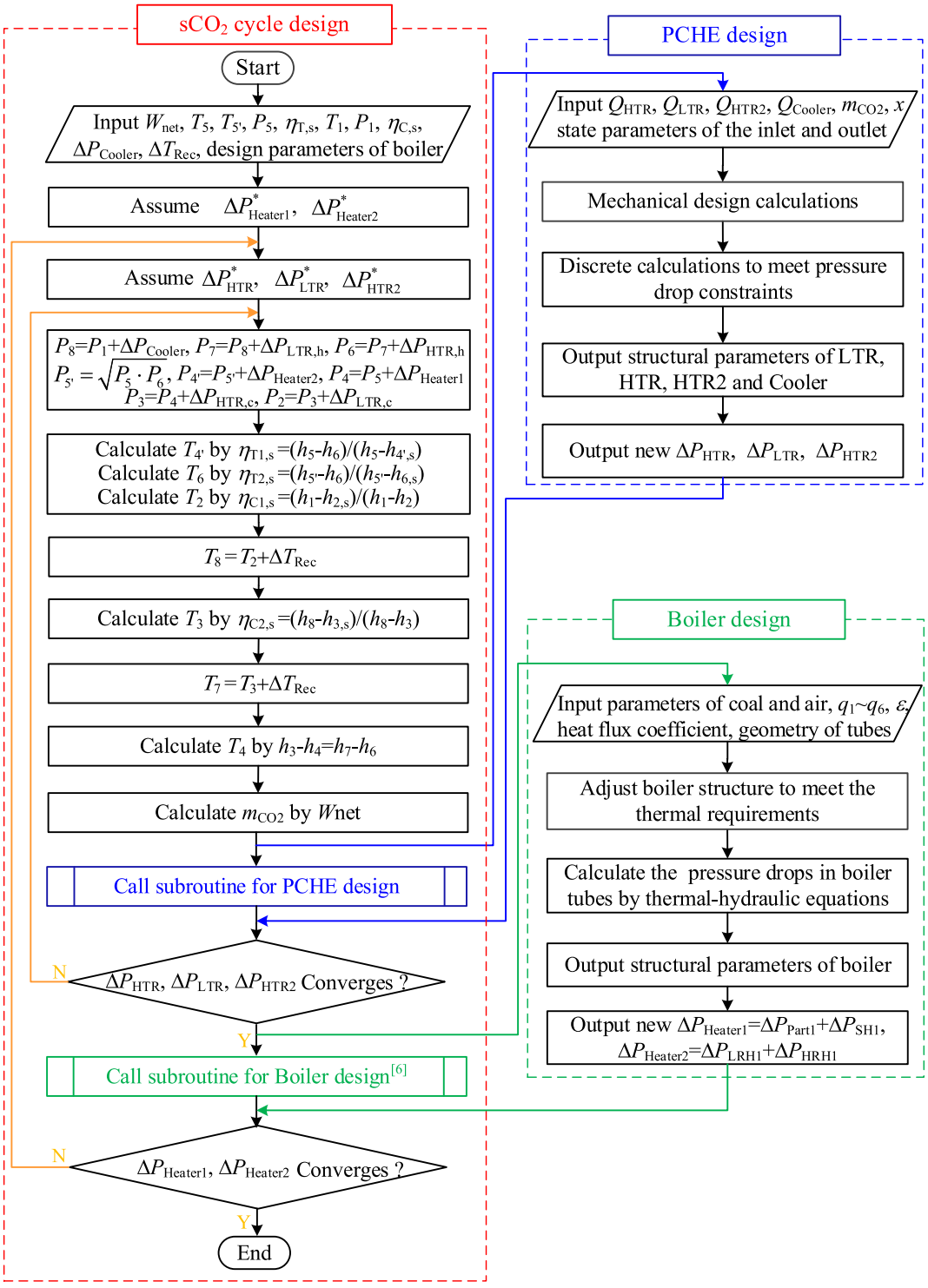

Fig. 4. Integrated design process of sCO_2 coal-fired power generation system and components.

[49] in terms of mass flow rate m, pressure ratio ε, speed N and isentropic efficiency η are transformed into the expressions of relative mass flow rate m_{re}, relative enthalpy rise ΔH_{re}, relative speed N_{re}, and relative efficiency η_{re} by using IGZ. Fig. 6a shows the performance curve for the main compressor C1 and Fig. 6b for the recompressor C2. The relative flow rate m_{re}, relative enthalpy rise ΔH_{re}, relative speed and relative efficiency η_{re} are calculated by:

$$m_{re}=\frac{m\sqrt{\gamma RZT}}{\gamma P}\Bigg/\left(\frac{m\sqrt{\gamma RZT}}{\gamma P}\right)_{design} \tag{27}$$

$$\Delta H_{re}=\frac{\Delta H}{\gamma RZT}\Bigg/\left(\frac{\Delta H}{\gamma RZT}\right)_{design} \tag{28}$$

$$N_{re}=\frac{N}{\sqrt{\gamma RZT}}\Bigg/\left(\frac{N}{\sqrt{\gamma RZT}}\right)_{design} \tag{29}$$

$$\eta_{re}=\eta/\eta_{design} \tag{30}$$

where P and T are compressor inlet pressure and temperature; ΔH is

Table 4
Main parameters of sCO_2 cycle at design condition.

State points	Pressure/MPa	Temperature/°C	Mass flow rate/kg/s
1	7.60	32.00	1467.59
2	31.20	82.46	1467.59
3	31.12	232.12	1904.45
4	30.95	504.79	1904.45
4a	30.85	352.66	273.30
4b	30.11	351.97	273.30
5	30.00	620.00	2177.75
4′	15.77	533.65	2177.75
5′	15.69	620.00	2177.75
6	8.20	535.45	2177.75
6b	8.15	453.22	183.35
7	8.00	242.10	2177.75
8	7.80	92.47	2177.75

Table 5
Design parameters of heater modules of sCO_2 boiler.

Heat exchange modules	$d_i \times \delta$ (mm)	d_o (mm).	s_1 (mm)	s_2 (mm)	A (m^2)	Heat absorption (MW)
Part1	24 × 8	40	56	–	850.11	112.55
Part2	24 × 8	40	56	–	651.64	112.55
H4b	20 × 6	32	45	–	20.41	29.97
SH	32 × 8	48	1350	60	919.54	55.46
HRH	35 × 5	45	450	60	3227.05	116.16
LRH	48 × 5.5	59	120	74	14209.04	116.16
H4a	48 × 5.5	59	120	74	43436.71	62.97
EAP	48 × 5.5	59	106	74	2253.72	17.81

Table 6
Design parameters of AP.

Item	hot segment	cold segment
Height h (mm)	1250.00	564.00
Flow area of flue gas F_g (m^2)	46.90	42.98
Flow area of primary air F_{a1} (m^2)	11.37	10.42
Flow area of secondary F_{a2} (m^2)	31.27	28.65
Heat transfer area A (m^2)	59311.63	21432.00
Heat transfer Q (MW)	62.79	17.29

Table 7
Design parameters of heat exchangers in the cycle.

Items	Cooler	LTR	HTR	HTR2
D_c (mm)	2.20	2.00	2.00	2.00
t_3 (mm)	0.36	0.94	1.10	1.10
t_2 (mm)	0.42	1.00	1.00	1.00
R_p	1	2	2	2
L_z (m)	1.27	1.47	1.28	0.53
L_x (m)	3.41	6.74	6.53	5.54
L_y (m)	3.04	6.00	7.20	5.40
ΔP_c (kPa)	22.16	80.77	174.35	150.00
ΔP_h (kPa)	200.00	200.00	200.00	277.65
A (m^2)	9550.7	26002.77	24942.52	654.64
Q_{th} (MW)	288.03	383.56	676.38	44.38

compressor enthalpy rise; γ is specific heat ratio; R is the gas constant; Z is compression factor; N is rotational speed; η is isentropic efficiency; subscripts 'design' and 're' indicate design condition parameters and relative parameters.

Taking the performance curve recompressor C2 shown in Fig. 6b as an example, the m_{re} and ΔH_{re} are calculated from Eqs. (27) and (28) with the given compressor mass flow rate m, inlet temperature T_{in}, inlet pressure P_{in}, and outlet pressure P_{out}. Then the operating point A is

Table 8
Technical parameters of turbomachines at the design condition.

Items	C1	C2	T1	T2
T_{in} (°C)	32.00	92.47	620.00	620.00
P_{in} (MPa)	7.60	7.80	30.00	15.69
T_{out} (°C)	82.46	232.12	533.65	535.45
P_{out} (MPa)	31.20	31.12	15.77	8.20
m (kg/s)	1467.59	710.16	2177.75	2177.75
η (%)	89.00	89.00	93.00	93.00
N (rpm)	3000	3000	3000	3000
W (MW)	57.22	73.92	216.98	214.15

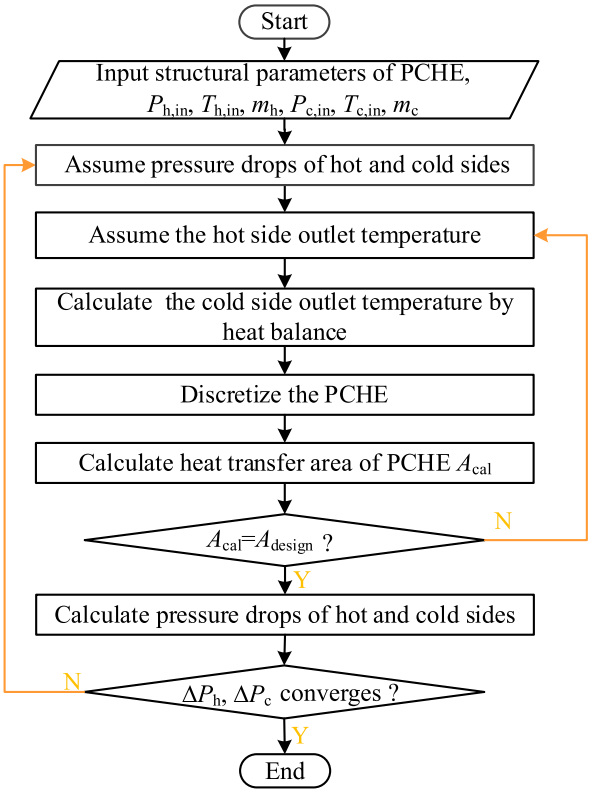

Fig. 5. Off-design calculation of PCHE.

determined, and the relative rotational speed N_{re} can be obtained by interpolation. According to N_{re} and m_{re}, the relative efficiency point A′ can be determined. Correspondingly, the actual efficiency of C2 can be obtained according to Eq. (30).

2.3.3. Off-design model of turbines

The rotational speed of the axial turbines is always kept constant in practice to ensure grid frequency stability. The sCO_2 turbine operates at a relatively low pressure ratio. The sCO_2 in the turbine behaves almost like an ideal gas. Thus, the Stodola ellipse method, a classical off-design model for axial turbines, can be used for the off-design calculation of the turbine [26,27,41,50,51]:

$$P_{in,od} = m_{in,od}^2 T_{in,od} Y_d + P_{out,od}^2 \tag{31}$$

$$Y_d = \frac{P_{in,d}^2 - P_{out,d}^2}{P_{in,d}^2 \varphi_d^2}, \varphi = m_{in}\frac{\sqrt{T_{in}}}{P_{in}} \tag{32}$$

$$\eta_{T,od} = \eta_{T,d} - 2\cdot\left(\frac{N_{od}}{N_d}\sqrt{\frac{\Delta H_{s,d}}{\Delta H_{s,od}}} - 1\right)^2 \tag{33}$$

where η_T is the turbine efficiency; ΔH is the enthalpy drop; N is the

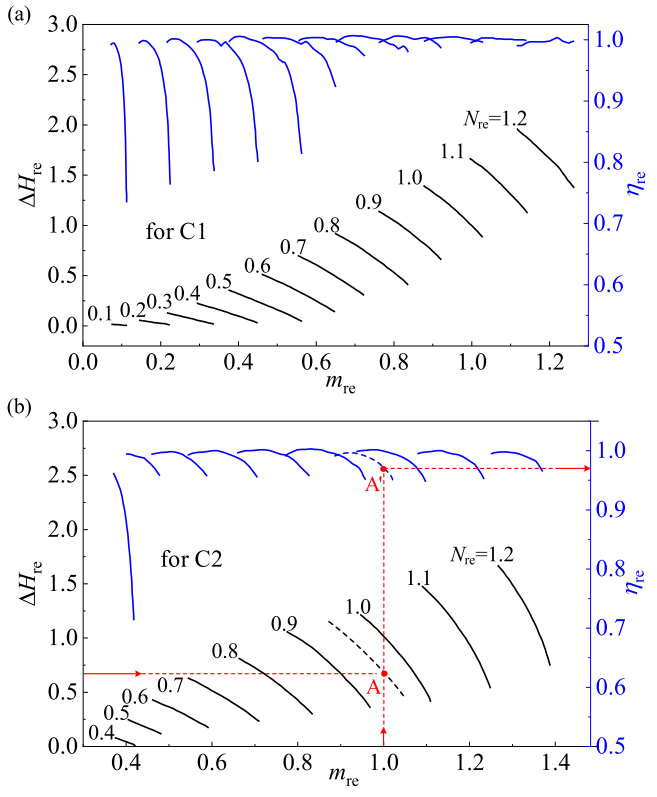

Fig. 6. Performance curves of main compressor and re-compressor.

turbine speed; the subscripts 'od' and 'd' denote off-design and design conditions; and 's' represents the isentropic process.

2.3.4. *Off-design model of sCO$_2$ boiler*

When the system is operated under variable loads, the excess air coefficient α, the air leakage coefficient $\Delta\alpha$, and the heat loss q_5 change with the boiler load [45,52]:

$$\begin{cases} \alpha_{od} = \alpha_d; \left(\dfrac{Q_{boiler,od}}{Q_{boiler,d}} \geq 0.7\right) \\ \alpha_{od} = \alpha_d + 0.7 - \dfrac{Q_{boiler,od}}{Q_{boiler,d}}; \left(\dfrac{Q_{boiler,od}}{Q_{boiler,d}} < 0.7\right) \end{cases} \tag{34}$$

$$\Delta\alpha_{od} = \Delta\alpha_d \left(\frac{Q_{boiler,d}}{Q_{boiler,od}}\right)^{0.5} \tag{35}$$

$$q_{5,od} = q_{5,d} \left(\frac{Q_{boiler,d}}{Q_{boiler,od}}\right) \tag{36}$$

The off-design calculation of boiler heating surfaces is shown in Fig. 7. Based on the given design structure parameters of heating surfaces and inlet parameters of the flue and sCO$_2$, the pressure drops of flue gas and sCO$_2$, and flue gas outlet temperature are assumed. Then the LMTD approach is carried out and the assumed flue gas outlet temperature $T_{fg,out}$ is iteratively adjusted to make the Q_{cal} converge to Q_{fg}. The pressure drops on both sides are calculated and compared to the initially assumed values, re-assuming the pressure drops to reduce their difference. when the pressure drops and heat load on both sides converge, the calculation is finished and the off-design parameters of boiler heating surfaces are obtained.

For the sCO$_2$ cycle black box model, the boiler structure parameter and detailed heat transfer process are not considered. It is assumed that the heat source can provide sufficient heat load to maintain the main gas and reheat temperature constant at any load ratio of the system. The

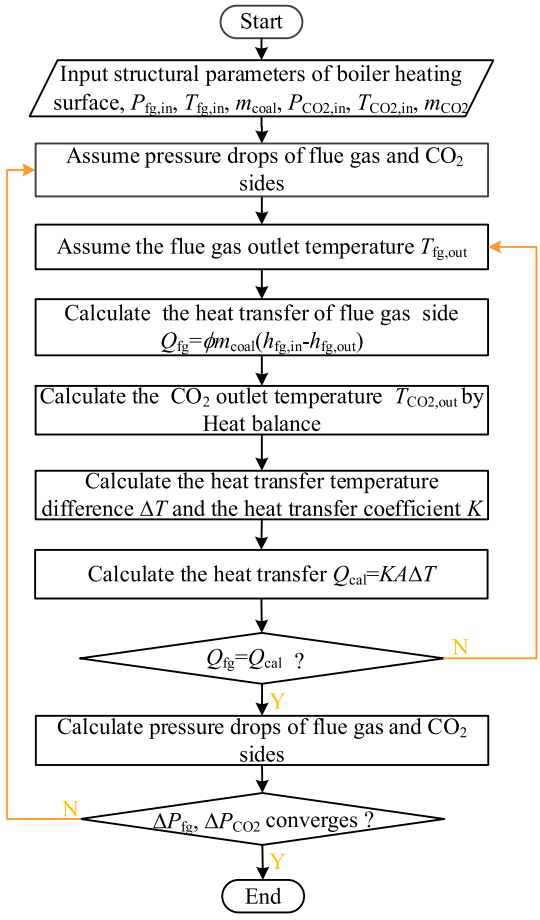

Fig. 7. Off-design calculation of boiler heating surface.

pressure drop of the CO$_2$ side in the heater is [53]:

$$\Delta P_{Heater,od} = \Delta P_{Heater,d} \left(\frac{m_{od}}{m_d}\right)^{7/4} \tag{37}$$

where $\Delta P_{Heater,d}$ is the heater design operating pressure drop; m_d and m_{od} are the sCO$_2$ mass flow rate through the heater at design conditions and off-design conditions.

2.4. *Partial load calculation process for SCPGS*

The SCPGS is equipped with an inventory tank (Fig. 1), whose inlet and outlet are connected to the highest pressure point (main compressor outlet) and the lowest pressure point (cooler outlet) of the system, respectively. Thus the pressure difference between the inventory tank and the outside can realize the storage and supplementation of CO$_2$ in the system during the regulation of the load. When the load decreases, valve V1 opens and the sCO$_2$ at the high-pressure point 2 enters the inventory tank to reduce the mass flow rate in the system. When the load increases, valve V2 opens and the sCO$_2$ in the inventory tank flows into the system through the low-pressure state point 1, increasing the system mass flow rate. The main gas temperature T_5 is maintained constant by changing the amount of coal during the variation of the system load ratio.

Fig. 8 shows the partial load calculation of the SCPGS: (1) Input the structural parameters of the components as well as the W_{net}, T_1, P_1, T_5, and the split ratios x; (2) Assume the boiler pressure drop ΔP^*_{boiler}, reheat temperature T^*_5 and the outlet temperature of heating surfaces T^*_c, T^*_{6b} and T^*_e; (3) Assume the mass flow rate of CO$_2$ m^*_{CO2} and the pressure drops of recuperators and cooler; (4) Call the off-design calculation

subroutine of T1 and T2; (5) Assume the outlet temperatures of recuperators T^*_{7a}, T^*_{7b} and T^*_8; (6) Call the off-design calculation subroutine of recuperators to obtain T_{7a}, T_{7b}, T_8 and pressure drops, and compare the assumed values in step (3) and step (5); (7) Calculate the mass flow rate m_{CO2} by the W_{net} and compare with the assumed values in step (3); If the residual criteria is satisfied, the off-design calculation is completed. (8) Determine the furnace heat load by the sCO_2 cycle parameters; (9) Assume the hot air temperature, exhaust flue gas temperature, coal consumption, and furnace outlet flue gas temperature; (10) Calculate the outlet temperatures of the flue gas and sCO_2 by the energy balance, and compare the predicted values with the assumed ones in step (9); If residual criteria is satisfied, the sCO_2 boiler off-design calculation is finished. (11) The boiler pressure drop ΔP_{boiler}, reheat temperature $T_{5'}$ and heated surface outlet temperatures T_c, T_{6b}, and T_e obtained from the sCO_2 boiler off-design calculation are calibrated against the assumed values in step (2), and a successful calibration completes the calculation of the SCPGS.

Fig. 9 gives the partial load calculation in the black box model of the SCPGS, which is similar to that in Fig. 8, with the difference that the reheat temperature $T_{5'}$ is given and assumed to be constant at any system load ratio, and the heater pressure drops are obtained directly by the system mass flow rate.

3. Results and discussion

3.1. Partial load operating characteristics of the SCPGS

The variation of the system thermal efficiency with load ratio for the sCO_2 black box model and the proposed SCPGS model are shown in Fig. 10. Various scholars have used the black box model to simulate the power systems [24,39], such as the traditional steam power unit and the solar thermal power system, however, it is rarely used for the sCO_2 coal-fired power system. In Fig. 10, it is seen that, for the black box model, the thermal efficiency first increases and then decreases with the load ratio decreasing from 100 % to 20 %, which is basically the same as the trend in our previous work [40] for the 300 MW sCO_2 RC power generation system. The mechanisms affecting the variation of the thermal efficiency have also been revealed [40]. Both positive and negative effects exist when the system is operating at partial load. The positive effects are caused by an increase in the recuperators effectiveness and the decrease of the pressure drops in each component, whereas the negative effects are brought on by the decrease of the main gas pressure and the turbine efficiency. The thermal efficiency is the trade-off of these two effects. The positive effect is greater than the negative effect when the system operates at 100%–80 % load ratio, thus the thermal efficiency is higher than the design thermal efficiency. The thermal efficiency reaches the maximum at 90 % load ratio. As the system load ratio drops into the range of 80%–20 %, the negative effects become more significant than the positive effect, and the thermal efficiency is lower than the design value.

As mentioned in Section 2, the black box model simplifies the heat transfer process in the boiler. By comparing the results predicted by the black box model and the present SCPGS model, the characteristics of the coal-fired sCO_2 power cycle can be better understood. In Fig. 10, the thermal efficiency of the SCPGS is lower than that of the black box model at the same load ratio, and it decreases monotonically as the load ratio decreases. The thermal efficiency decreases from 51.07 % at the design point to 36.07 % at 20 % load ratio. And the lower the load ratio is, the larger the difference between the SCPGS and the black box model exhibits, with a maximum difference of 0.85 % at 20 % load ratio.

The efficiency gap between SCPGS and the black box model is caused by the simplification of the heat transfer in the sCO_2 boiler. In the sCO_2 black box model, it is assumed that the heat source can provide the required heat load for the system at any load ratio and keep the main gas temperature and reheat temperature constant as the design point. Thus, the black box model is suitable for some specific heat sources, such as the solar thermal energy. The molten salt mass flow rate in the solar receiver can be adjusted to ensure the same molten salt temperature enters the thermal storage tank, and the main gas and reheat temperatures can be kept constant at the design values by adjusting the molten salt mass flow rate into the intermediate heater [24]. However, for the SCPGS, the high temperature flue gas will pass through each specific heating surface in the sCO_2 boiler to heat the sCO_2. The main stream outlet temperature can be guaranteed to be unchanged by adjusting the boiler coal consumption when the load ratio changes. In this condition, the reheat stream should passively absorb the remaining flue gas heat, consequently, it cannot maintain the design reheat temperature.

As shown in Fig. 11a, the reheat temperature of the black box model remains constant at 620 °C while the reheat temperature of SCPGS decreases with decreasing load ratio [36]. In SCPGS, the reheat temperature changes at a faster rate from 100 % to 70 % load rate. At 80 % load rate, the reheat temperature has deviated from the design value by more than 10 °C down to 608.85 °C. From 70 % to 20 % load ratio, the reheat temperature is reduced moderately and reaches 597.93 °C at 20 % load ratio, deviating from the design value by more than 30 °C. However, when the main stream and reheat temperatures deviate too much from the design value, it will not only cause thermal stresses that shorten the unit's service life and affect its safety, but also have an impact on the system's efficiency. so it is usually necessary to control the variation of the main stream and reheat temperatures within ±5–10 °C [45].

As is shown in Fig. 11b, the lower reheat temperature $T_{5'}$ of the SCPGS model leads to the lower outlet temperature of turbine 2 (T2), T_6, compared to that of the black box model. Consequently, the main heater inlet temperature, T_4, of the SCPGS model is also lower than that of the black box model after the regenerator. Fig. 11c illustrates the change of heat loads of the main heater and reheater with load ratios. In the SCPGS, due to the larger temperature rise (T_5-T_4) of the CO_2, the heat load in main heater, $Q_{Main\text{-}Heater}$, is larger than the black box model. However, the lower reheat temperature $T_{5'}$ of the SCPGS makes its reheater heat load, $Q_{Re\text{-}Heater}$, smaller than that of the black box model. And the total heat absorption ($Q_{Main\text{-}Heater} + Q_{Re\text{-}Heater}$) of the SCPGS is larger than that of the sCO_2 black box model generation system at the same load ratio. Fig. 11d shows that the larger total heat absorption ($Q_{Main\text{-}Heater} + Q_{Re\text{-}Heater}$) makes the system heat absorption per unit mass flow rate of CO_2 q_{total} of the SCPGS is larger than that of the black box model system.

Fig. 12a shows that the reduction of isentropic efficiency of T1, η_{T1}, is quite limited, especially for the system load ratio larger than 40 %, while the isentropic efficiency of T2, η_{T2}, has a gradual decrease within the system load ratio 100%–50 % and a significant decrease for the load ratio lower than 50 %. The trend of these results is the same as that of the RC + RH power generation system with radial turbines and radial compressors in the literature [24], implying that the characteristics of sCO_2 cycle at partial load are basically similar, regardless of whether axial turbomachine or radial turbomachine is used. In addition, it is seen that at the same load ratio, the decrease in reheat temperature $T_{5'}$ in the SCPGS also makes η_{T2} smaller than that of the black box model, and their difference becomes larger as the system load ratio decreases. Consequently, the specific work, w_{net}, of SCPGS is smaller than that of the black box model (Fig. 12b). Considering the lower q_{total} of SCPGS in Fig. 11d and the efficiency formula $\eta_{th} = w_{net}/q_{total}$, the smaller thermal efficiency of SCPGS in Fig. 10 can be evidenced.

3.2. Partial load operation characteristics of the sCO_2 boiler

The above discussion of results in Figss. 10–12 reveals the decrease in the reheat temperature $T_{5'}$ in the SCPGS while keeping the main gas temperature T_5 constant, which cannot be reflected in the black box model. The partial load characteristics of the sCO_2 boiler will have a direct impact on the safety and economy of the SCPGS. Therefore, it is necessary to study the partial load operation characteristics of the sCO_2 boiler to further optimize the partial load performance of the SCPGS.

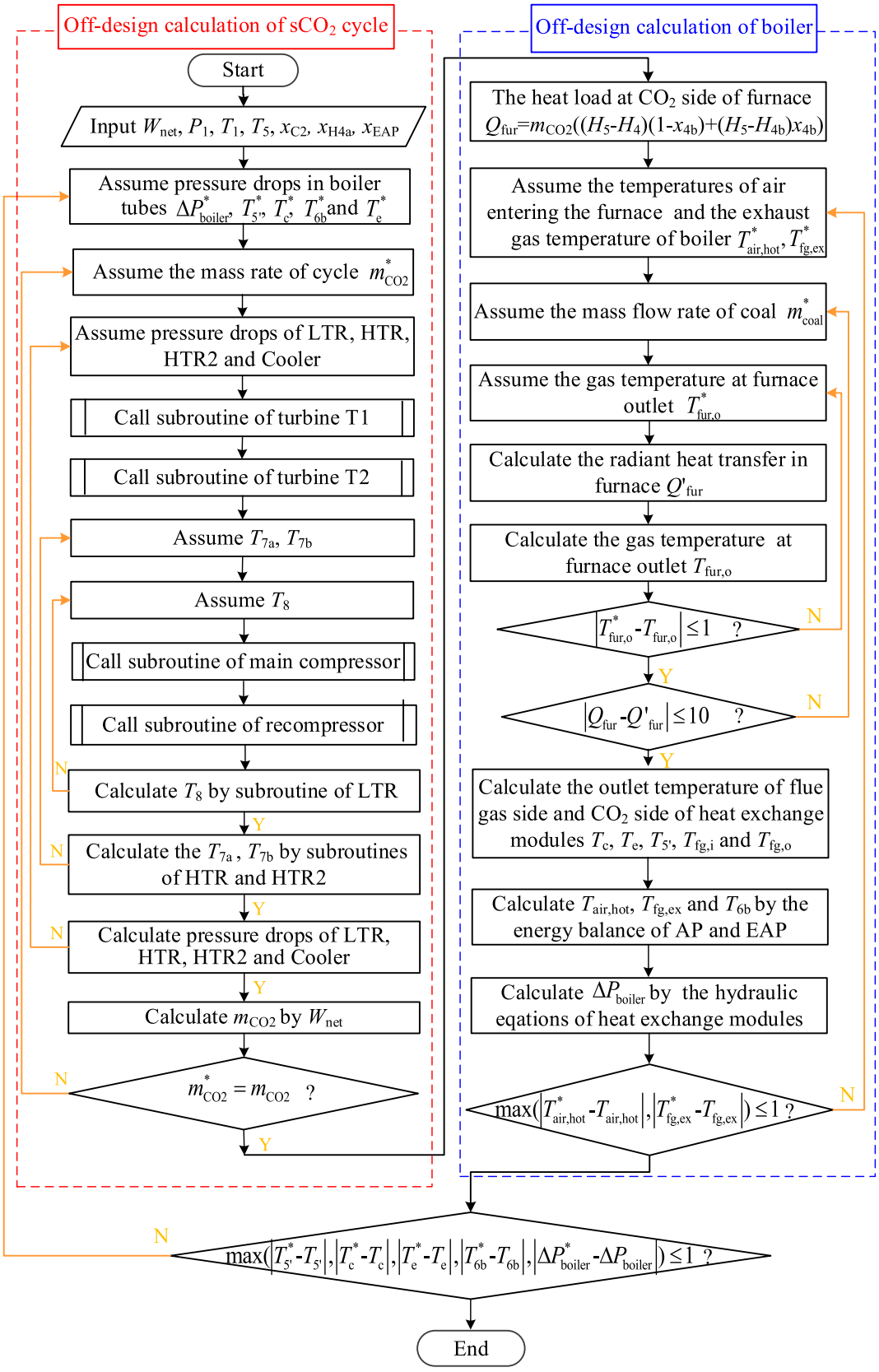

Fig. 8. Partial load calculation process for SCPGS.

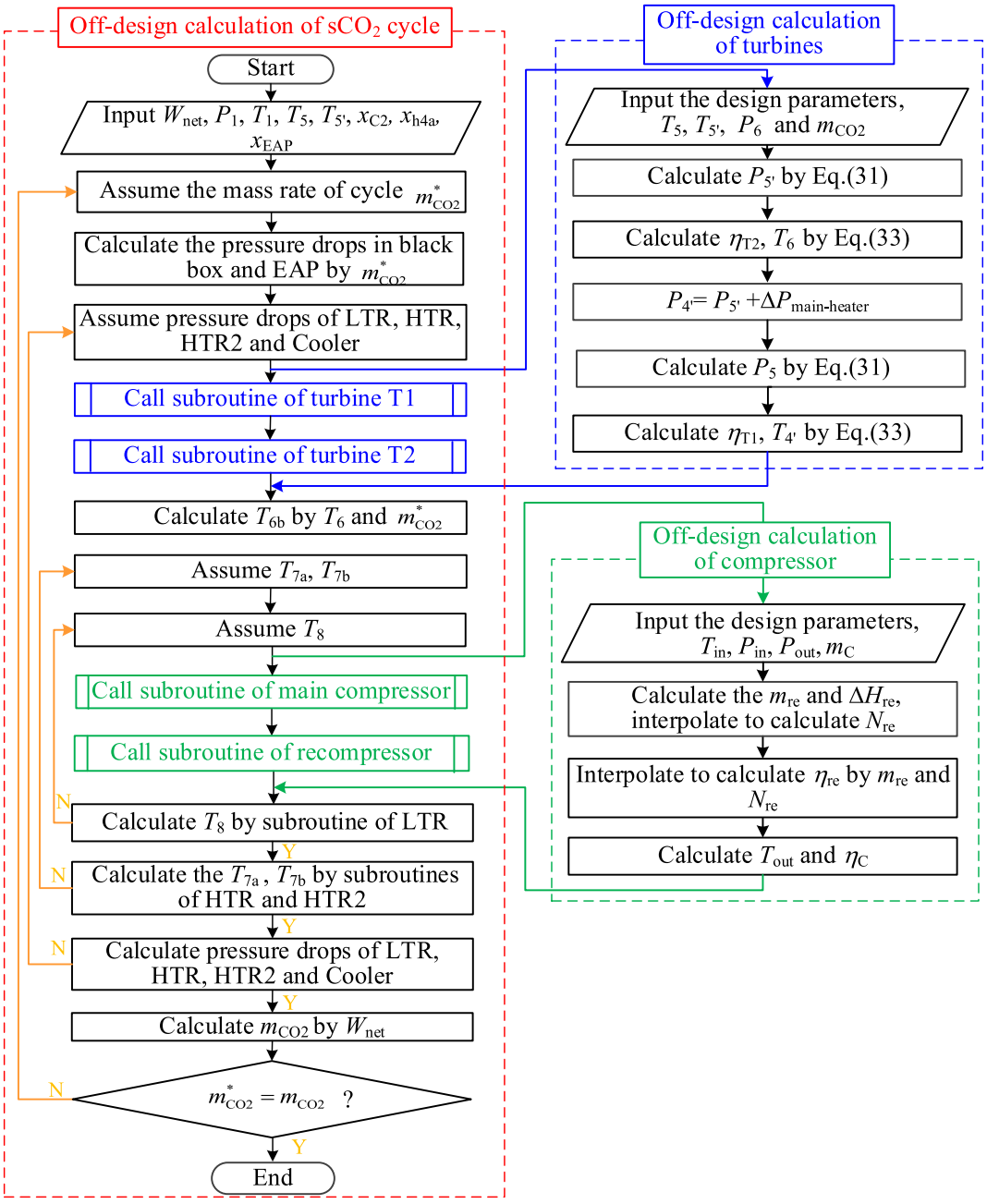

Fig. 9. Partial load calculation process for sCO_2 black box model power generation system.

The heat transfer in the sCO_2 boiler is quite different from that of the heat exchangers in the cycle as it has two mechanisms: radiation heat transfer and convection heat transfer. The furnace outlet serves as the boundary between radiation and convective heat transfer. As depicted in Fig. 13a, the radiation heating surfaces Part1, Part2, SH, and H4b are arranged in the furnace, and the convective heating surfaces HRH, LRH, H4a, and AP are installed after the furnace outlet. Therefore, in SCPGS, the main heater and the reheater are mainly the radiant heating surfaces and convective heating surfaces respectively. The coal consumption decreases approximately in equal proportion with the reduction of load ratio, and the flame temperature in the furnace decreases less, so that the change of the radiant heat transfer is smaller. While for convection heating surface, the flue gas temperature and flue gas flow rate decrease at the same time when coal consumption decreases, which makes the convection heat transfer temperature difference and the heat transfer coefficient of the flue gas side are reduced, so the convection heat transfer in the boiler decreases more. Consequently, the proportion of radiant heat transfer in the sCO_2 boiler increases as the load ratio decreases (Fig. 13b), so the reheat temperature will decrease in the condition that the main steam temperature remains unchanged. It is noted that the proportion of radiation heat transfer decreases slightly when the system load ratio is reduced from 70 % to 60 %. The main reason is that the flue gas volume becomes higher as the excess air coefficient α in the boiler starts to increase when the load ratio is reduced below 70 % (see Fig. 12c). The increasing excess air coefficient α also makes the decrease in reheat temperature more gradual, as discussed in Fig. 10a, thus the adjustment of the excess air coefficient can play a role to regulate the ratio of radiant heat load and the reheat temperature [36]. In addition, the furnace outlet flue gas temperature $T_{fg,o}$ and the exhaust flue gas temperature $T_{fg,ex}$ both decrease with the decreasing load ratio due to the decreases of coal consumption.

For the sCO_2 boiler, the boiler efficiency is mainly affected by the

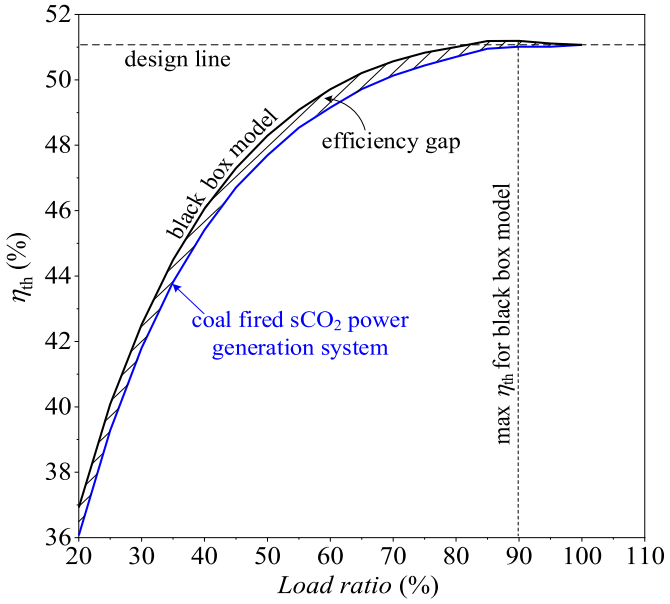

Fig. 10. Variation trend of thermal efficiency with load ratio predicted by the black box model and the proposed SCPGS model.

heat losses due to the exhaust gas q_2 and the radiation q_5. As shown in Fig. 13c, q_5 keeps increasing with decreasing load ratio while the trend of q_2 is more complicated. It is determined by both the exhaust flue gas temperature $T_{fg,ex}$ and the excess air coefficient α. $T_{fg,ex}$ decreases with the decreasing load ratio (Fig. 13b), which tends to reduce the q_2. As α remains unchanged at 100%–70 % load ratio and becomes higher at 70%–20 % load ratio. The trade-off between these two factors makes q_2 decreases at 100%–65 % load ratio, then gradually increases at 65%–50 % load ratio, and finally decreases again at 50%–20 % load ratio. Because of the combined effect of q_2 and q_5, the sCO_2 boiler efficiency η_b reaches its maximum value at 70 % load ratio (Fig. 13d), which is basically consistent with the trend of steam boiler efficiency in the literature [54]. The generation efficiency η_e is the product of η_{th}, η_b, pipe efficiency η_p, and mechanical efficiency η_g. $\eta_p = 0.99$ and $\eta_g = 0.985$ are applied in this work. It is seen that η_e decreases with the decreasing load ratio, and declines more quickly at the lower load ratio. At 20 % load ratio, η_e decreases from the design value of 47.05 %–33.33 %, and the coal consumption rate per kW·h of electrical energy increases from 316.29 g/kW·h to 447.13 g/kW·h.

3.3. Regulation of the SCPGS operation

The main heater heat load is dominated by radiation heat transfer while the reheat heat load is dominated by convection heat transfer. Thus, improving the ratio of radiation to convection heat absorption of the boiler to increase the sCO_2 reheat temperature is the key to the SCPGS efficiency optimization. In addition, a large deviation of sCO_2 reheat temperature from the design value will seriously affect the safety of the unit. Therefore, the reheat temperature of the system needs to be adjusted from both economic and safety points of view.

For steam coal-fired units with the reheating process, the common reheat temperature adjustment methods are [45]: (1) flue gas side: flue gas recirculation [55], adjust flue gas baffle [56], adjust burners angle [57], etc.; (2) process side: steam bypass, spray attemperation, etc. [56]. For the sCO_2 boiler in this paper, the flue gas recirculation can be carried out in the subsequent modification. The method of adjusting the flue gas baffle cannot be adopted either because the main heating surfaces and reheating surfaces are not arranged parallel. Therefore, for the present structure of the sCO_2 boiler, we consider the following two methods to control the reheat temperature: (1) adjusting burners angle: This method

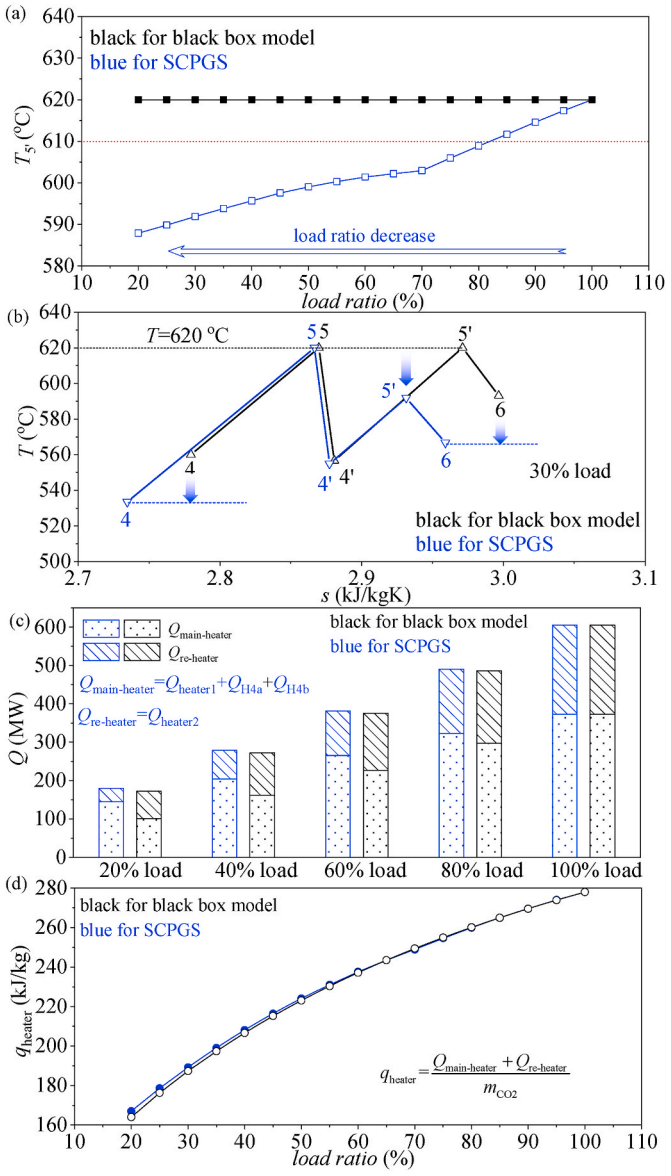

Fig. 11. The change of (a) reheat temperature, (b)*T-s* diagram of heating and expansion processes, (c) heater heat, and (d) q_{heater} with load ratio.

regulates the proportion of radiation and convection heat transfer in the boiler by changing the flame center height determined by the angle of the swing burner; (2) changing the sCO_2 split ratio: Similar to the steam bypass in the traditional steam boiler, changing the mass flow ratio of the working fluid flowing through the heating surfaces to achieve the adjustment of the reheat temperature. In the present work, the objective is to control the reheat temperature within a deviation of ±10 °C from the design value [58]. The minimum system load ratio corresponding to the lowest reheat temperature, which is 10 °C lower than the design value, is defined as the minimum safe load ratio (MSLR). The available system load ratio and the related thermal efficiency of the SCPGS are calculated and analyzed.

3.3.1. Adjust the burners angle

In this paper, the swing burner is used in sCO_2 boiler. Fig. 14a shows the schematic diagram of the swing burner, which can be adjusted up and down and the maximum swing angle is $\beta = \pm 30^{o}$ [45]. When the burner angle is positive, the flame center position rises and the amount of heat transfer in the furnace decreases as the flame's residence time in the furnace shortens, which can make the radiation heat transfer of the

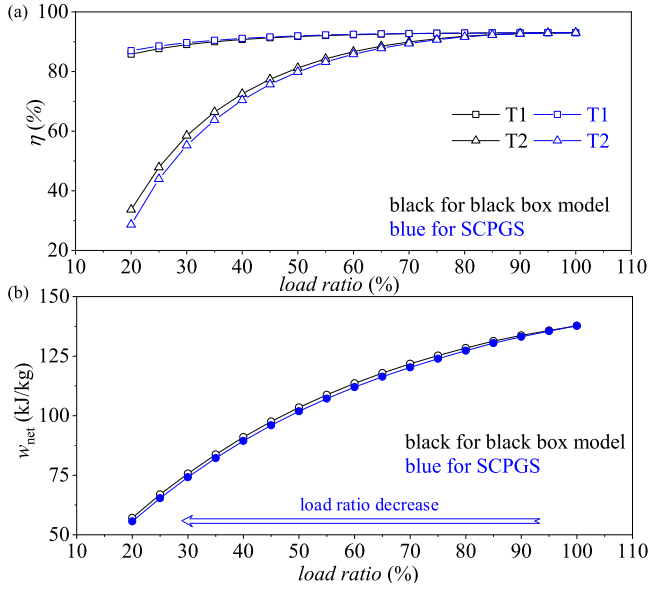

Fig. 12. The change of (a)turbine efficiencies , and (b) w_{net} with load ratios.

boiler decrease and the convective heat transfer increase. Fig. 14b shows the change of the proportion of radiant heat transfer with the load ratio at the burners angle of 20° and the reference case. It is seen that the proportion of radiant heat is obviously reduced when the burner angle is adjusted to 20°. In this paper, all the adjustment measures in this paper are only adopted at partial load, Thus, $\beta = 0°$ is applied at 100 % load ratio. The reference case is exactly the heat proportion in Fig. 13b.

The change in the proportion of radiant and convective heat transfer brought about by the adjustment of the burner angle will have an impact on the performance of the system. Fig. 15a illustrates that when the burner angle is adjusted to 20°, the increase in the proportion of convective heat transfer increases the work done in T2 to improve the thermal efficiency of the system η_{th}. However, the flue gas flow is shortened as the flame center position rises, which increases the exhaust flue gas temperature $T_{fg,ex}$. The exhaust loss q_2 increases as $T_{fg,ex}$ rises and this reduces the boiler efficiency η_b. Meanwhile, the elevated flame center also increases the furnace outlet temperature $T_{fur,o}$. In order to prevent slagging at the furnace and convection heating surfaces, the $T_{fur,o}$ should be lower than the softening temperature (ST) of the coal [45], in this work, ST = 1190 °C. Fig. 15b shows that $T_{fur,o}$ will be higher than ST at the load ratio between 80 % and 100 % when $\beta = 20°$, which is easy to coke and slag in the boiler and will cause uneven heating and high-temperature burst of the tubes, thus threatening the safety of the unit. Therefore, 80%–100 % load ratio is signed as the slagging range. Besides, for the $\beta = 20°$ case, although the reheat temperature $T_{5'}$ is higher than the reference case in Fig. 11, the reheat temperature still deviates from the design value by more than 10 °C when the load ratio is lower than 60 %. Thus, the 60%–20 % load ratio is still in the low reheat temperature range. As a result, the normal working range of the system is 80%–60 % load ratio. Fig. 15c shows that the slagging range is extended to 75%–100 % load ratio and the low reheat temperature range shrinks to 45%–20 % load ratio when the burner angle is adjusted to the maximum of 30°. The 75%–45 % load ratio is the normal working range. It is noted that the reheat temperature at 95 % load ratio will exceed the design value by more than 10 °C and enter the reheat temperature overheat range, which also poses a threat to the safety of the unit. In conclusion, raising the burner angle can raise the reheat temperature and lower MSLR, but it will also increase the $T_{fur,o}$ at high loads, making the heating surface more susceptible to coking and slagging. Additionally, the slagging range is wider and MSLR is lower as the burner angle increases.

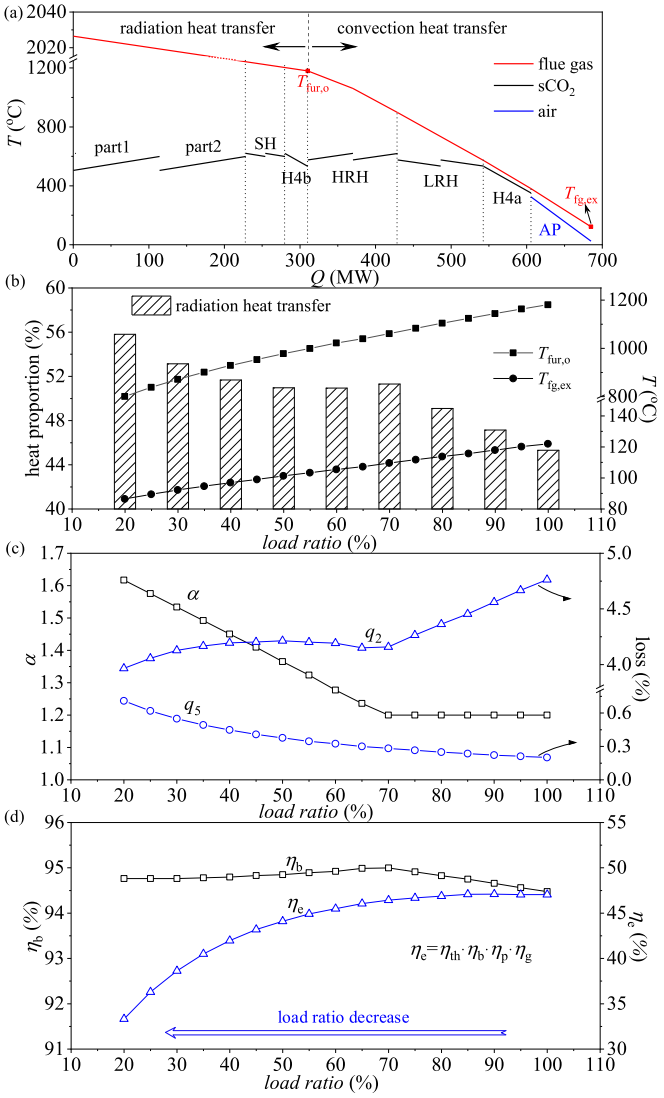

Fig. 13. Partial load operating characteristics of sCO_2 boiler (a: boiler *T-Q* diagram at design condition, b: heat proportion, $T_{fur,o}$ and $T_{fg,ex}$, c: α and loss coefficients, d: η_b and η_e).

3.3.2. *Change the split ratios*

As is shown in Fig. 16a, there are three split points: the state points 8, 3a, and 6 in the present SCPGS. At split point 8, part of the sCO_2 (x_{C2}·m_{CO2}) enters the C2, and the other ((1-x_{C2})·m_{CO2}) enters the Cooler. The total mass flow rate through split point 3a is (1-x_{C2})·m_{CO2}, and the amount of sCO_2 enters HTR2 is x_{H4a}·m_{CO2}. The rest of sCO_2 ((1-x_{C2}-x_{H4a})·m_{CO2}) enters the HTR cold side to absorb heat. The split point 6 is located at the outlet of T2. After splitting, a portion of sCO_2 (x_{EAP}·m_{CO2}) enters the EAP to heat the secondary air, and the remainder ((1-x_{EAP})·m_{CO2}) flows through the HTR hot side to heat the cold side fluid.

In this paper, x_{C2}, x_{H4a}, and x_{EAP} denote the ratio of the mass flow rate of sCO_2 through the recompressor, H4a, and EAP to the total mass flow rate, respectively. The design value of x_{C2}, x_{H4a}, and x_{EAP} are 0.33, 0.13, 0.09, respectively. Δx_{C2}, Δx_{H4a} and Δx_{EAP} denote the difference between x_{C2}, x_{H4a}, x_{EAP} and their design values, respectively. When the value of Δx is negative, it indicates that the split ratio is smaller than the design value, which means that the mass flow rate through the corresponding components is reduced. Changing the split ratios of sCO_2 has little effect on the flue gas temperature at the furnace outlet, and there is no slagging range when the load is reduced. Consequently, the main focus is its effect on MSLR. In order to ensure the pinch point

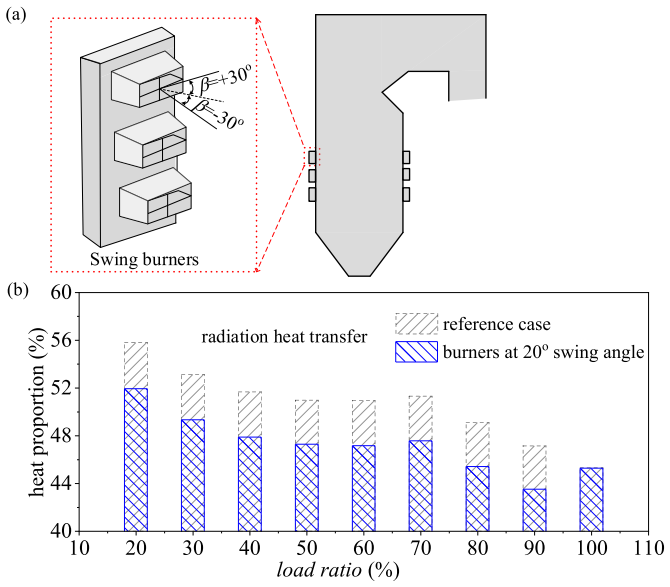

Fig. 14. Effect of adjusting burners angle on boiler heat transfer.

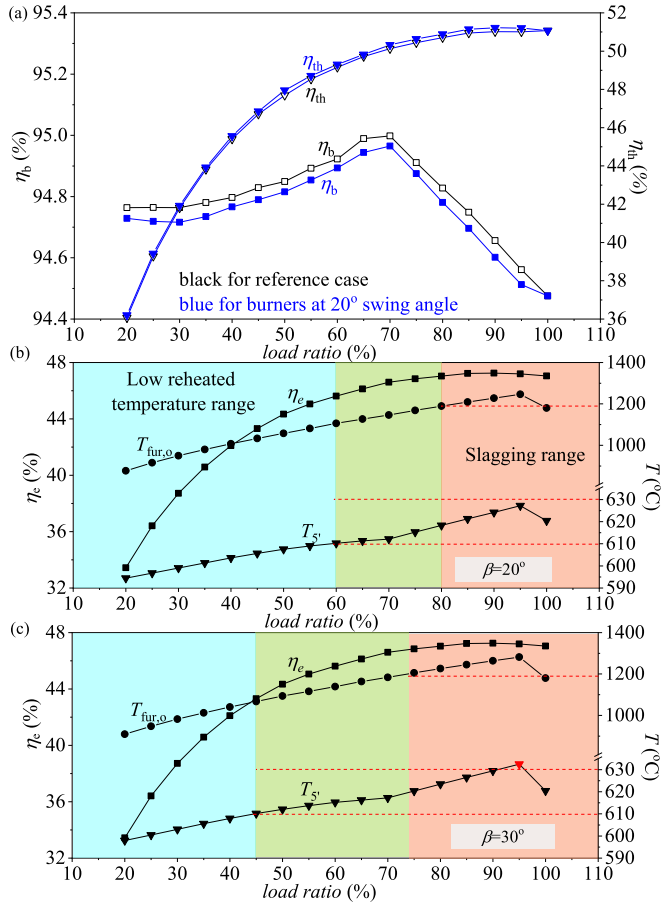

Fig. 15. Effect of adjusting burner angle on the SCPGS.

temperature difference of recuperators is within an appropriate range [36], the maximum variation of each split ratio is set as ±0.08. Fig. 16b shows the variation of the MSLR when the split ratios x_{C2} is changed. The MSLR remains unchanged for $\Delta x_{C2} = -0.02$~-0.08, while it decreases to 80 % for $\Delta x_{C2} = -0.07$~-0.03 and to 75 % for $\Delta x_{C2} = -0.08$, indicating that the decrease in the split ratio x_{C2} has a positive effect on

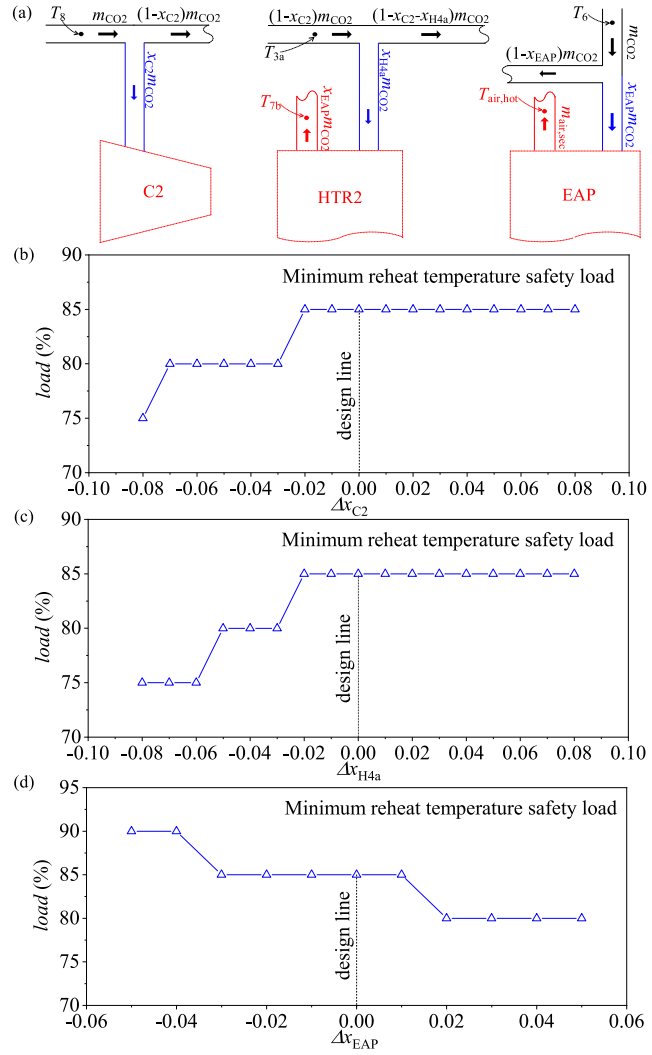

Fig. 16. Effect of changing split ratios on the SCPGS.

raising the reheat temperature $T_{5'}$ to expand the normal working range of the unit. As is shown in Fig. 16c, the effect of the split ratio x_{H4a} on the MSLR is similar to that of x_{C2}. The MSLR remains unchanged for $\Delta x_{H4a} = -0.02$~0.08, and decreases to 80 % for Δx_{H4a} = -0.05~-0.03, and to 75 % for $\Delta x_{H4a} = -0.08$~-0.06. The effect of the split ratio x_{EAP} on the MSLR is different from x_{C2} and x_{H4a}. Fig. 16d indicates that MSLR increases when x_{EAP} decreases, reducing the normal working range of the boiler. The MSLR rises to 90 % for $\Delta x_{EAP} = -0.05$~-0.04, to 85 %, 80 % and 75 % for $\Delta x_{EAP} = -0.03$~0.01, Δx_{EAP} = 0.02–0.07, and Δx_{EAP} = 0.08, respectively. It is temporarily concluded that decreasing x_{C2} and x_{H4a}, and increasing x_{EAP} can decrease MSLR, thereby increasing the normal working range of the system.

In addition, the change in the split ratios also affects the system generation efficiency η_e, as shown in Fig. 17. According to the above analysis, the split ratio changes of $\Delta x_{C2} = -0.05$, $\Delta x_{H4a} = -0.05$ and $\Delta x_{EAP} = 0.05$ are selected. It is seen that the η_e at the same load ratio is lower than the reference case for these split ratio changes, which is mainly because changing the split ratio increases the reheat temperature by increasing the coal consumption through the increase of the heat required by the CO_2 in the radiant heat transfer surface. Taking account of the results in Fig. 15 that adjusting the burners angle can increase η_e and reduce MSLR to 45 %, we can see that the priority should be given to adjusting the burner angle when controlling the reheat temperature. For the change of the split ratios, the η_e at lower load ratio is more important. Fig. 17 shows that $\eta_{e,\Delta xEAP = 0.05} > \eta_{e,\Delta xH4a = -0.05} > \eta_{e,\Delta xC2=-0.05}$ at

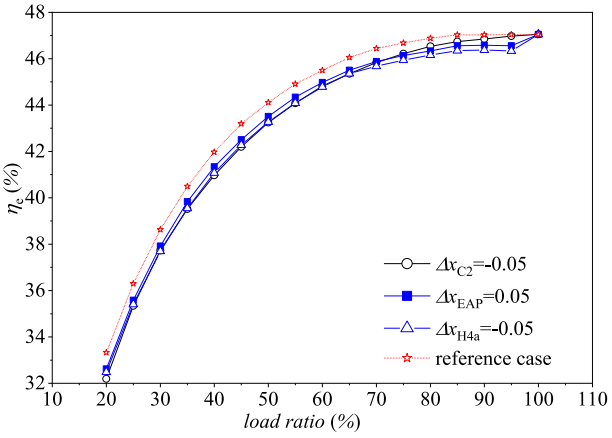

Fig. 17. Effect of changing split ratios on power generation efficiency of the SCPGS.

lower load ratios, thus, when adjusting the split ratios, priority should be given to the x_{EAP}.

3.3.3. *Comprehensive control strategy*

The results in Section 3.3.1 proved the feasibility of increasing the burners angle and adjusting the split ratios to reduce the MSLR of the system. However, for a single adjustment measure, the MSLR is 45 % at burners angle of 30° and 75 % at most for adjusting the split ratio, which implies that neither of these two methods can meet the deep peak regulation requirements of the SCPGS. Will adjusting the burner angle and split ratios at the same time further reduce the MSLR? How does the η_e of the system change at the same time? In this section, the comprehensive control strategy of adjusting the burners angle and split ratios simultaneously is explored to achieve deep peak regulation of the SCPGS.

Fig. 18a–c shows the variation of key parameters of the SCPGS with load ratio when the burners angle is adjusted to 30° and the split ratios are adjusted separately. Fig. 18a shows that, compared with Fig. 15c, the slagging range remains unchanged while the MSLR decreases from 45 % to 35 % for the case of $\beta = 30^{o}$ and Δx_{C2} = -0.08. However, the reheat-temperature-overheat-range increases to 85%–95 % load ratio. Fig. 18b illustrates that for the cases of $\beta = 30^{o}$ with $\Delta x_{H4a} = -0.08$, the low reheat temperature range is 20%–35 % load ratio, the normal working range is 35%–70 % load ratio, and the slagging range is 70%–100 % load ratio. At 85%–95 % load ratio, $T_{5'}$ is higher than 630 °C, which makes SCPGS enter the reheat-temperature-overheat-range. As is shown in Fig. 18c, for the cases of $\beta = 30^{o}$ with $\Delta x_{EAP} = 0.08$, the low reheating temperature range, normal working range and slagging range, the reheat-temperature-overheat-range, are 20%–35 %, 35%–70 %, 70%–100 % and 85%–95 % load ratio, respectively. It is seen that the burner angle of 30° and the single split ratio adjustment of 0.08 both reduce the MSLR to 35 %, and the η_e decreases compared to only adjusting the burner angle. Fig. 18d shows that $\eta_{e,\Delta xEAP = 0.08} > \eta_{e,\Delta xH4a = -0.08} > \eta_{e,\Delta xC2=-0.08}$ at lower load ratio, which is similar to the results in Fig. 17.

The combined regulation of adjusting the burner angle to 30° and changing a single split ratio can reduce the MSLR to 35 %. To further reduce the MSLR, the combined control strategy of adjusting the burner angle and changing multiple split ratios are studied, and the variations of key system parameters are shown in Fig. 19. It is seen in Fig. 19a that, under the conditions of $\beta = 30^{o}$, $\Delta x_{EAP} = 0.08$, and $\Delta x_{H4a} = -0.08$, the MSLR can be reduced to 25 % load ratio while the slagging range is increased to 65%–100 % load ratio and the reheat-temperature-overheat-range is increased to 75%–95 % load ratio. Further, as shown in Fig. 19b, under the conditions of $\beta = 30^{o}$, $\Delta x_{EAP} = 0.08$, $\Delta x_{H4a} = -0.08$, and $\Delta x_{C2} = -0.08$, the MSLR of the system can be reduced to 20 %, which can fully satisfy the deep peak regulation requirement of

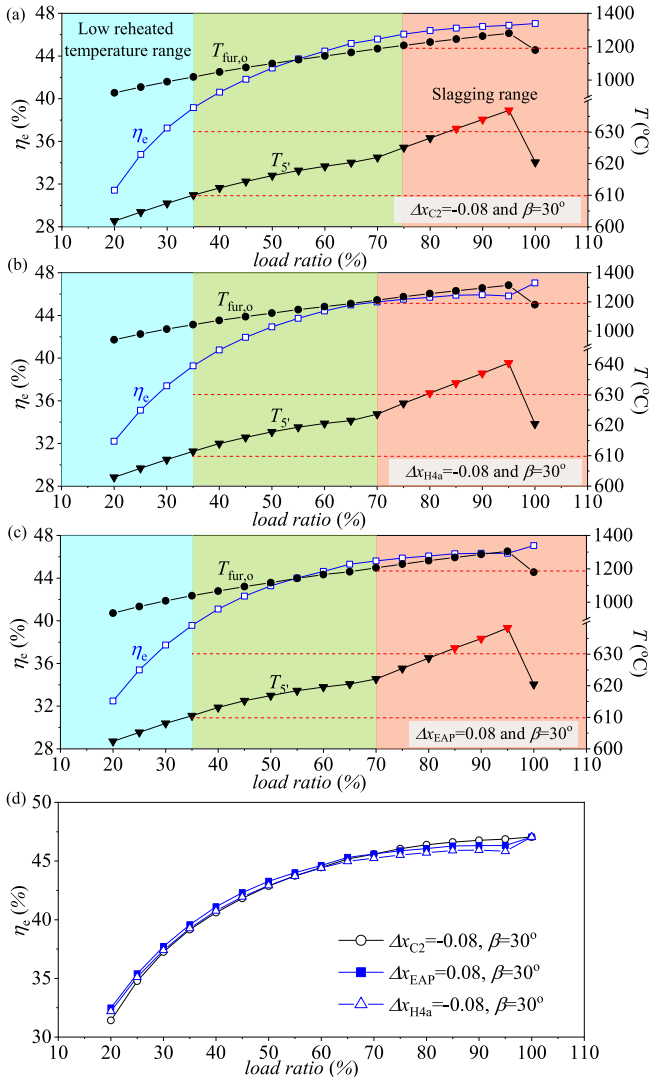

Fig. 18. Effect of changing split ratios on the SCPGS under the condition of 30° burner angle.

the SCPGS. However, it also has an increased slagging range of 65%–100 % load ratio and the reheat temperature overheat range becomes more severe, 70%–95 % load ratio.

Adjusting the burner angle upward can improve the power generation efficiency and reduce the MSLR, but it will increase the slagging range, thus it is not appropriate for the high load ratio. Changing the split ratios can reduce the MSLR and η_e, and when combined with adjusting the burner angle, it also increases the slagging range and the reheat temperature overheat range, which is more suitable for the low load ratio. As is shown in Fig. 19c, considering the feature of these two regulation methods, we propose a comprehensive control strategy to enable the SCPGS to achieve deep load regulation efficiently and safely: at 100%–85 % load ratio, no regulation is applied to the system; at 85%–45 % load ratio, the reheat temperature is regulated by gradually adjusting the burner angle upward β = 0-30°; at 45%–20 % load ratio, the burner angle is set to 30° and the system split ratios are changed (x_{EAP}, x_{H4a}, x_{C2} in order) so that the unit can operate safely at lower load ratio. Compared with the no regulation case, η_e is higher at 85%–45 % load ratio by only adjusting the burners angle for reheat temperature regulation, and is lower at 45%–20 % load ratio when starting to adjust the split ratios.

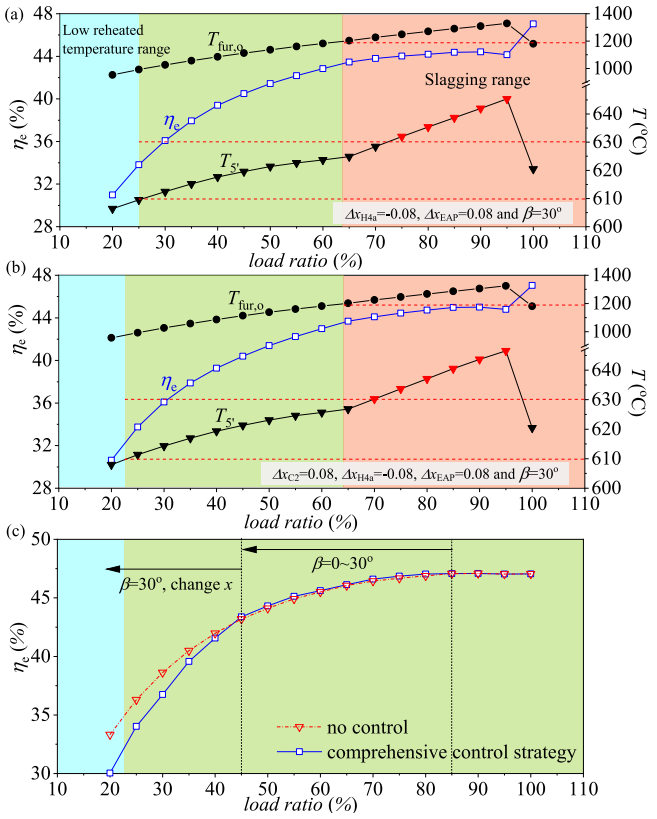

Fig. 19. Comprehensive control strategy of the SCPGS.

4. Conclusion

In this work, a comprehensive steady-state model of a 300 MW sCO_2 coal-fired power generation system was developed by fully considering the heat transfer processes of the heating surfaces in the boiler. The partial load operating characteristics and the control strategies to regulate the reheat temperature are investigated and the main findings are summaries as follows.

(1) The black box model will overestimate the thermal efficiency of the system as its simplification of the heat transfer processes in the boiler cannot predict the reduction of reheat CO_2 temperature in partial load operation. The reduced reheat temperature leads to the reduction of T2 outlet temperature and the boiler inlet temperature, which increases the heat absorption per unit mass flow rate of CO_2. It also decreases the isentropic efficiency of T2. These two aspects result in the lower system thermal efficiency.

(2) Under partial load operation, the proportion of radiative heat transfer of the sCO_2 boiler increases with the decreasing load ratio, and both the furnace outlet temperature $T_{fur,o}$ and the exhaust flue gas temperature $T_{fg,ex}$ decrease. These temperatures and the excess air coefficient α influence the exhaust heat loss q_2 and the radiation heat loss q_5, which makes the boiler efficiency η_b reach the maximum at 70 % load ratio. Under the effect of η_b and η_{th}, the power generation efficiency η_e decreases with the decreasing load ratio.

(3) Two regulation methods are proposed and simulated through the SCPGS model: adjusting the swing burner angle and changing the split ratios under the constraint of ±10 °C deviation of reheat temperature from the design point. Swinging the burner angle upward can reduce the minimum reheat temperature safety load ratio from 85 % to 45 % and improve the system power generation efficiency while the drawback is the high furnace outlet temperature will make the heating surface easy to coke and slag at high load ratios. Changing a single split ratio can increase the normal operation range from 85%-100 % to 75%–100 %, but it will reduce the system power generation efficiency.

(4) Considering the safety and economy of the SCPGS, a comprehensive control strategy is developed: at 100%–85 % load ratio, no regulation of the system is applied; at 85%–45 % load ratio, the reheat temperature is regulated by adjusting the burner angle upward; at 45%–20 % load ratio, the burners angle is set as 30° and the split ratios are changed in the order of x_{EAP}, x_{H4a}, and x_{C2}. This control strategy enables the SCPGS to achieve a wide load regulation (20%–100 %) efficiently and safely to meet the deep peak regulation requirements.

CRediT authorship contribution statement

Haonan Zheng: Investigation, Methodology, Software, Writing – original draft. **Zheng Miao:** Conceptualization, Methodology, Writing – review & editing. **Jinliang Xu:** Conceptualization, Funding acquisition, Supervision, Writing – review & editing.

Declaration of competing interest

We state that the manuscript titled as "Partial load operation characteristics of supercritical CO_2 coal-fired power generation system" by Haonan Zheng, Zheng Miao and Jinliang Xu does not have any conflict of interest including any financial, personal or other relationships with other people or organizations within three years of beginning the submitted work that could inappropriately influence, or be perceived to influence, the present work.

Data availability

Data will be made available on request.

Acknowledgements

The authors are grateful to the National Natural Science Foundation of China (Nos. 52130608, 51776064, 51821004) for their assistance.

References

[1] Energy, climate change and environment 2016. Paris: IEA; 2016.
[2] Xi J. Statement at the general debate of the 75th session of the united Nations general assembly. http://www.xinhuanet.com/english/2020-09/23/c_139388686.htm.
[3] Si N, Zhao Z, Su S, Han P, Sun Z, Xu J, et al. Exergy analysis of a 1000 MW double reheat ultra-supercritical power plant. Energy Convers Manag 2017;147:155–65.
[4] Blum R, Bugge J, Kjaer S. USC 700 C power technology—a European success story. VGB PowerTech 2009;4:26–32.
[5] Sulzer G. Verfahren zur erzeugung von arbeit aus warme. Swiss Patent; 1950, 269599.
[6] Liu C, Xu J, Li M, Wang Z, Xu Z, Xie J. Scale law of sCO2 coal fired power plants regarding system performance dependent on power capacities. Energy Convers Manag 2020;226:113505.
[7] Feher EG. The supercritical thermodynamic power cycle. Energy Convers 1968;8:85–90.
[8] Angelino G. Real gas effects in carbon dioxide cycles. Atomkernenergie 1971;17:27–33.
[9] Utamura M. Thermodynamic analysis of part-flow cycle supercritical CO2 gas turbines. J Eng Gas Turbines Power 2010:132.
[10] Kato Y, Nitawaki T, Muto Y. Medium temperature carbon dioxide gas turbine reactor. Nucl Eng Des 2004;230:195–207.
[11] Muto Y, Ishiyama S, Kato Y, Ishizuka T, Aritomi M. Application of supercritical CO2 gas turbine for the fossil fired thermal plant. J Energy Power Eng 2010;4.
[12] Dostal V, Driscoll MJ, Hejzlar P. A supercritical carbon dioxide cycle for next generation nuclear reactors. Massachusetts Institute of Technology, Department of Nuclear Engineering; 2004.
[13] Sarkar J, Bhattacharyya S. Optimization of recompression S-CO2 power cycle with reheating. Energy Convers Manag 2009;50:1939–45.
[14] Chacartegui R, Muñoz De Escalona JM, Sánchez D, Monje B, Sánchez T. Alternative cycles based on carbon dioxide for central receiver solar power plants. Appl Therm Eng 2011;31:872–9.

[15] Besarati SM, Yogi Goswami D. Analysis of advanced supercritical carbon dioxide power cycles with a bottoming cycle for concentrating solar power applications. J Sol Energy Eng 2014:136.
[16] Sun E, Xu J, Li M, Li H, Liu C, Xie J. Synergetics: the cooperative phenomenon in multi-compressions S-CO2 power cycles. Energy Convers Manag X 2020;7:100042.
[17] Sun E, Xu J, Hu H, Li M, Miao Z, Yang Y, et al. Overlap energy utilization reaches maximum efficiency for S-CO2 coal fired power plant: a new principle. Energy Convers Manag 2019;195:99–113.
[18] Duniam S, Veeraragavan A. Off-design performance of the supercritical carbon dioxide recompression Brayton cycle with NDDCT cooling for concentrating solar power. Energy 2019;187:115992.
[19] Neises T. Steady-state off-design modeling of the supercritical carbon dioxide recompression cycle for concentrating solar power applications with two-tank sensible-heat storage. Sol Energy 2020;212:19–33.
[20] Singh R, Miller SA, Rowlands AS, Jacobs PA. Dynamic characteristics of a direct-heated supercritical carbon-dioxide Brayton cycle in a solar thermal power plant. Energy 2013;50:194–204.
[21] Chen R, Romero M, González-Aguilar J, Rovense F, Rao Z, Liao S. Design and off-design performance comparison of supercritical carbon dioxide Brayton cycles for particle-based high temperature concentrating solar power plants. Energy Convers Manag 2021;232:113870.
[22] Wang X, Li X, Li Q, Liu L, Liu C. Performance of a solar thermal power plant with direct air-cooled supercritical carbon dioxide Brayton cycle under off-design conditions. Appl Energy 2020;261:114359.
[23] Dyreby JJ, Klein SA, Nellis GF, Reindl DT. Modeling off-design and part-load performance of supercritical carbon dioxide power cycles. In: Turbo expo: power for land, sea, and air. American Society of Mechanical Engineers; 2013. V8T–34T.
[24] Yang J, Yang Z, Duan Y. Part-load performance analysis and comparison of supercritical CO2 Brayton cycles. Energy Convers Manag 2020;214:112832.
[25] Li H, Fan G, Cao L, Yang Y, Yan X, Dai Y, et al. A comprehensive investigation on the design and off-design performance of supercritical carbon dioxide power system based on the small-scale lead-cooled fast reactor. J Clean Prod 2020;256:120720.
[26] Fan G, Dai Y. Thermo-economic optimization and part-load analysis of the combined supercritical CO2 and Kalina cycle. Energy Convers Manag 2021;245:114572.
[27] Fan G, Li H, Du Y, Chen K, Zheng S, Dai Y. Preliminary design and part-load performance analysis of a recompression supercritical carbon dioxide cycle combined with a transcritical carbon dioxide cycle. Energy Convers Manag 2020;212:112758.
[28] Ahn Y, Kim MS, Lee JI. S-CO2 cycle design and control strategy for the SFR application. In: Proceedings of the 5th international symposium–supercritical CO2 power cycles; 2016. p. 28–31. San Antonio, TX, USA.
[29] Sathish S, Kumar P, Nassar A. Analysis of a 10 MW recompression supercritical carbon dioxide cycle for tropical climatic conditions. Appl Therm Eng 2021;186:116499.
[30] Alfani D, Astolfi M, Binotti M, Macchi E, Silva P. Part-load operation of coal fired sCO2 power plants. In: 3rd European supercritical CO2 conference september 19-20. Paris: France; 2019. p. 1–9. 2019.
[31] Alfani D, Astolfi M, Binotti M, Macchi E, Silva P. Optimization of the part-load operation strategy of sCO2 power plants. 5th International Seminar on ORC Power Systems; 2019. p. 1–10.
[32] Zhou J, Zhu M, Su S, Chen L, Xu J, Hu S, et al. Numerical analysis and modified thermodynamic calculation methods for the furnace in the 1000 MW supercritical CO2 coal-fired boiler. Energy 2020;212:118735.
[33] Fleming D, Holschuh T, Conboy T, Rochau G, Fuller R. Scaling considerations for a multi-megawatt class supercritical CO2 Brayton cycle and path forward for commercialization. In: Turbo expo: power for land, sea, and air. American Society of Mechanical Engineers; 2012. p. 953–60.
[34] Bai W, Zhang Y, Yang Y, Li H, Yao M. 300 MW boiler design study for coal-fired supercritical CO2 Brayton cycle. Appl Therm Eng 2018;135:66–73.
[35] Li P, Zhong W, Chen X, Liu X. Heat distribution and boiler efficiency of 600MW coal-fired CFB boiler with S-CO2 power cycle. Proceedings of the CSEE 2019;39:2080–92 [in Chinese].
[36] Tong Y, Duan L, Pang L. Off-design performance analysis of a new 300 MW supercritical CO2 coal-fired boiler. Energy 2021;216:119306.
[37] Sun E, Xu J, Li M, Liu G, Zhu B. Connected-top-bottom-cycle to cascade utilize flue gas heat for supercritical carbon dioxide coal fired power plant. Energy Convers Manag 2018;172:138–54.
[38] Xu J, Sun E, Li M, Liu H, Zhu B. Key issues and solution strategies for supercritical carbon dioxide coal fired power plant. Energy 2018;157:227–46.
[39] Peng S, Wang Z, Hong H, Xu D, Jin H. Exergy evaluation of a typical 330MW solar-hybrid coal-fired power plant in China. Energy Convers Manag 2014;85:848–55.
[40] Zheng H., Xu J., Wang Z., Miao Z. Study on partial load operation characteristics of sCO2 Cycle. Sci Sin Tech 2024: 54(1): 78–90.[in Chinese].
[41] Hu H, Liang S, Jiang Y, Guo C, Guo Y, Zhu Y, et al. Thermodynamic and exergy analysis of 2 MW S-CO2 Brayton cycle under full/partial load operating conditions. Energy Convers Manag 2020;211:112786.
[42] Jiang Y, Liese E, Zitney SE, Bhattacharyya D. Design and dynamic modeling of printed circuit heat exchangers for supercritical carbon dioxide Brayton power cycles. Appl Energy 2018;231:1019–32.
[43] Chu W, Li X, Ma T, Chen Y, Wang Q. Experimental investigation on SCO2-water heat transfer characteristics in a printed circuit heat exchanger with straight channels. Int J Heat Mass Tran 2017;113:184–94.
[44] Le Pierres R, Southall D, Osborne S. Impact of mechanical design issues on printed circuit heat exchangers. In: Proceedings of SCO2 power cycle symposium. University of Colorado Bolder; 2011.
[45] Che D. Boilers: theory, design and operation. Xi'an Jiaotong University Press; 2008.
[46] Gou J, Wang W, Ma C, Li Y, Lin Y, Li H. Numerical simulation of the performance of an axial compressor operating with supercritical carbon dioxide. In: International conference on nuclear engineering. American Society of Mechanical Engineers; 2018. V8T–9T.
[47] Pelton R, Jung S, Allison T, Smith N. Design of a wide-range centrifugal compressor stage for supercritical CO2 power cycles. J Eng Gas Turbines Power 2018:140.
[48] Jeong Y, Son S, Cho SK, Baik S, Lee JI. A Comparison study for off-design performance prediction of a supercritical CO2 compressor with similitude analysis. In: Fluids engineering division summer meeting. American Society of Mechanical Engineers; 2019. V3A.
[49] Wang Y, Guenette G, Hejzlar P, Driscoll M. Compressor design for the supercritical CO2 Brayton cycle. 2nd International Energy Conversion Engineering Conference; 2004. p. 5722.
[50] Ma Y, Morosuk T, Liu M, Liu J. Development and comparison of control schemes for the off-design operation of a recompression supercritical CO2 cycle with an intercooled main compressor. Energy 2020;211:119011.
[51] Ray A. Dynamic modelling of power plant turbines for controller design. Appl Math Model 1980;4:109–12.
[52] Alfani D, Astolfi M, Binotti M, Silva P. Part load strategy definition and annual simulation for small size sCO2 based pulverized coal power plant. In: Proceedings of ASME turbo expo 2020. London, England: ASME; 2020. V11T–31T.
[53] Dyreby JJ. Modeling the supercritical carbon dioxide Brayton cycle with recompression. The University of Wisconsin-Madison; 2014.
[54] Madejski P, Żymełka P. Calculation methods of steam boiler operation factors under varying operating conditions with the use of computational thermodynamic modeling. Energy 2020;197:117221.
[55] Zhang G, Xu W, Wang X, Yang Y. Sensitivity analysis and optimization of a coal-fired power plant in different modes of flue gas recirculation. Energy Proc 2014;61:2114–7.
[56] Liu H, Yu P, Xue J, Deng L, Che D. Research and application of double-reheat boiler in China. Processes 2021;9:2197.
[57] Fan H, Xu W, Zhang J, Zhang Z. Steam temperature regulation characteristics in a flexible ultra-supercritical boiler with a double reheat cycle based on a cell model. Energy 2021;229:120701.
[58] Tong Y, Duan L, Pang L. Design optimization of a new S-CO2 single reheat coal-fired boiler. J Eng Thermophys 2021;42:314–25 [in Chinese].

Nomenclature

A: area, m^2
c_p: specific heat capacity, kJ/(kgK)
C: compressor
ct: enthalpy value of cold air per unit volume, kJ/m^3
D: diameter, mm
f: friction coefficient
h: specific enthalpy, kJ/kg; heat transfer coefficient, W/m^2KH
L: length, m
m: mass flow rate, kg/s
N: rotating speed, rpm; number of sub-heat exchanger
P: pressure
q: heat transfer per unit mass, kJ/kg; heat loss percentage of boiler, %
Q: thermal load, MW; heating value of coal or flue gas, kJ/kg
RC: recompression cycle
RH: Reheating
Rp: ratio between the number of hot and cold plates
RS: stress, MPa
t: Thickness, mm
T: temperature
U: overall heat transfer coefficient, $kW/m^2/K$
UA: heat conductance, kJ/K
V: volume, m^3
w: work done per unit mass flow rate, kJ/kg
x: split ratio of flow rate
Z: gas compressibility

Subscripts

1, 2, 3 …: state points of cycle
c: channel or cold side
d: design conditions
ex: exhaust
fg: flue gas
fur: furnace
h: hot side; hydraulic
in: input or inlet
od: off-design
out: outlet
p: plate
re: relative
s: isentropic

th: thermal
x, y, z: coordinates
specific enthalpy, kJ/kg: Greek symbols
α: excess air coefficient
ε: emissivity
ΔT: temperature difference, ^{o}C
ΔP: pressure difference, ^{o}C
γ: ratio of specific heat capacity
η: efficiency
ρ: density, kg/m^3
φ: boiler heat retention coefficient
gas constant,J/kgK: Abbrevations
AP: air preheater
C1: main compressor
C2: auxiliary compressor
EAP: external air preheater
HRH: high temperature reheater
HTR: high temperature regenerative heat exchanger
H4a: Heater 4a
H4b: Heater 4b
LMTD: logarithmic mean temperature difference
LTR: low temperature regenerative heat exchanger
MSLR: minimum safe load ratio
sCO_2: supercritical carbon dioxide
SCPGS: supercritical carbon dioxide coal-fired power generation system
SH: superheater
T1: high pressure turbine
T2: low pressure turbine
V1-2: valve 1-2